#### **RESEARCH PAPER**



# Topology optimisation for rotor-stator fluid flow devices

Eduardo Moscatelli<sup>1</sup> · Diego Hayashi Alonso<sup>1</sup> · Luís Fernando Nogueira de Sá<sup>1</sup> · Renato Picelli<sup>1,2</sup> · Emílio Carlos Nelli Silva<sup>1</sup>

Received: 17 November 2021 / Revised: 14 March 2022 / Accepted: 17 March 2022 / Published online: 15 April 2022 © The Author(s), under exclusive licence to Springer-Verlag GmbH Germany, part of Springer Nature 2022

#### **Abstract**

Multi-component devices such as flow machines, heat exchangers, and electric motors present parts with different physical properties and operating in different states. Optimisation algorithms may improve the performance of these devices, and the simultaneous optimisation of a set of parts may harness the interaction of these parts to generate improved designs. Particularly, rotating flow devices such as pumps and turbines present rotating and stationary components. If a description of the fluid flow between the rotating and stationary parts is desired, it is necessary to model solid at different velocities. However, the standard topology optimisation formulation for fluid flow problems considers only a single stationary solid or a single rotating solid in a rotating reference frame. Thus, this work proposes a topology optimisation formulation capable of solving fluid flow problems with different solid velocities. The idea is to add mutually exclusive Darcy terms to the linear momentum equation. Each Darcy term models a different rotation and only one term may be active at each element. The method uses two discrete design variable fields. The moving limits of the optimisation algorithm are adjusted to handle the two discrete design variable fields, and extra constraints are added to ensure proper phase transitions. The algorithm is applied to two design problems: a Tesla pump and a labyrinth seal. The governing equations are solved by the Finite Element Method, and the optimisation is solved by an approach based on the Topology Optimisation of Binary Structures (TOBS) algorithm, with each linearized subproblem being solved through integer linear programming with a branch-and-bound algorithm.

**Keywords** Topology optimisation  $\cdot$  2D swirl flow  $\cdot$  Rotor-stator design  $\cdot$  Discrete design variables  $\cdot$  Integer linear programming  $\cdot$  FEniCS

# 1 Introduction

Devices such as pumps, turbines, heat exchangers, and electric motors present components with different physical properties and operating in different states (e.g., velocity and temperature). One approach for improving the performance of these devices is to consider optimisation algorithms, which may be applied to individual parts of the device or to a set of parts simultaneously. The advantage of simultaneously

Responsible Editor: Xiaojia Shelly Zhang

- ⊠ Eduardo Moscatelli emoscatelli@usp.br
- Department of Mechatronics and Mechanical Systems Engineering, Polytechnic School of the University of São Paulo, São Paulo, Brazil
- Department of Naval Architecture and Ocean Engineering, Polytechnic School of the University of São Paulo, São Paulo, SP, Brazil

optimising a set of parts is to harness the interaction between them to improve performance. In this case, the description of each component and the interaction between them must be included in the modelling to enable simultaneous optimisation. For example, if the optimisation algorithm is applied to the rotor and stator of a flow machine simultaneously, it is necessary to describe rotating and stationary parts. This work will focus on this application.

There are multiple approaches for optimising a device and this work is concerned with the topology optimisation method, which consists of dividing the design domain into elements and delegating to an optimisation algorithm the task of choosing the material of each element. Particularly, the application of topology optimisation to fluid flow problems started with Borrvall and Petersson (2003) and was extensively developed (Alexandersen and Andreasen 2020).

Regarding the design of flow machines by topology optimisation, Romero and Silva (2014) proposed a method to design rotors of bladed flow machines. They optimised



the channels between the blades of the rotor using a multiobjective function based on energy dissipation, vorticity, and delivered (turbine) or consumed (pump) power. A rotating reference frame is used to solve the Navier–Stokes equations. Then, Sá et al. (2018) presented the complete development cycle of a bladed small-scale pump with a design approach based on the work of Romero and Silva (2014). The authors of Sá et al. (2018) designed, manufactured, and tested the pumps verifying the improved performance obtained by applying topology optimisation. Alonso et al. (2019) proposed a topology optimisation formulation to design the rotor of a Tesla pump. The 2D swirl flow model was used in a rotating reference frame. The authors introduced an extension of the material model to treat the inverse permeability as a matrix which enables assigning different permeabilities for radial, tangential and axial velocity components. They also introduced a new term to vorticity objective function to reduce the grayscale level. Okubo et al. (2021) applied the continuous adjoint approach in topology optimisation to design the rotor flow paths in 3D. Cyclic boundary conditions were used to represent the repeating patterns and the power dissipation is minimized. All these works optimised the rotor by considering a rotating domain, meaning that the influence of the stationary parts is not considered. Therefore they did not need to represent the differences in velocity between the rotor and stator. However, if a simultaneous optimisation of the rotor and the stator is desired, it is necessary to use different velocities for the rotor and stator. To the best knowledge of the authors, the first work capable of considering different velocities for rotor and stator during topology optimisation is presented by Sá et al. (2022), where a differential equation is used to propagate the rotating boundary condition to solid elements connected to the rotating wall.

The majority of works on fluid flow topology optimisation consider one fluid phase and one solid phase. Recently, some researchers also made contributions to multiphase fluid flow topology optimisation to address problems that are better described by more than one fluid phase due to differences in physical properties. Tawk et al. (2019) proposed a topology optimisation formulation to design heat exchangers with two different fluids separated by a solid phase. The authors used two design variable fields and a multi-material interpolation scheme inspired by the work of Bendsøe and Sigmund (1999). Then, Høghøj et al. (2020) presented a topology optimisation approach to design two-fluid heat exchangers by considering only one design variable field and erosiondilatation techniques to guarantee the separation between the different fluid phases. Kobayashi et al. (2021) also presented a density-based topology optimisation method with one design variable field to design two-fluid heat exchangers. The idea of the authors was to define the phases in terms of the design variables in such a way that the solid phase is always present between different fluid phases.

In this work, fluid flow problems are also addressed with three material phases in topology optimisation. However, instead of considering two fluid phases, two solid phases at different rotations are studied. The idea is to consider the relative rotating motion between the rotor and the stator during the topology optimisation of flow machines and their components. The proposed method can distribute both solid phases freely in the design domain or can be restricted to place solid only at some locations. The effectiveness of the proposed method is demonstrated by solving two design problems: a Tesla pump and a labyrinth seal. The used topology optimisation approach is a modified version of Topology Optimisation of Binary Structures (TOBS) introduced by Sivapuram and Picelli (2018) and extended to fluid flow by Souza et al. (2021). The modifications proposed in this work are the inclusion of two discrete design variable fields and extra constraints to control material phase changes. Also, a modification to the Navier-Stokes equation is made to include two mutually exclusive Darcy terms.

This paper is organized as follows. In Sect. 2, the physical problem is stated with the modifications necessary for considering fluid flow topology optimisation with two solid phases at different velocities. Also, the necessary modifications to describe three phases with two discrete design variable fields are presented. In Sect. 3, the numerical methods and software tools used to implement the proposed algorithm are described. In Sect. 4, results obtained with the proposed formulation and different parameters are presented. Finally, Sect. 5 closes the study with conclusions and discussions.

### 2 Rotor-stator formulation

The problems considered in this work present symmetry around an axis, so cylindrical coordinates and axisymmetry are considered to reduce the computational cost of the numerical solution (2D swirl flow model). Figure 1 illustrates the relation between the coordinates of a Cartesian frame  $O_{xyz}$  and a cylindrical frame  $O_{r\theta z}$ . The cylindrical reference frame may be fixed or rotating. If the cylindrical reference frame is rotating, it is a non-inertial reference frame and additional body forces appear in the momentum equations. In this work, one example is solved in a rotating reference frame whilst the other example is solved in a fixed reference frame. The objective is to show the proposed model and algorithm in both conditions of the reference frame.

This work considers steady-state, incompressible, Newtonian, and low Reynolds fluid flow in the absence of gravitational forces. The stress tensor for a Newtonian fluid is given by



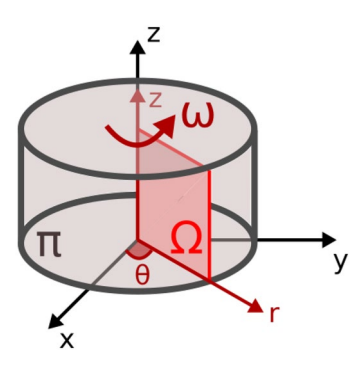


Fig. 1 Illustration of a Cartesian  $(O_{xyz})$  and a cylindrical  $(O_{r\theta z})$  coordinate systems

$$\sigma(\mathbf{v}, p) = -p\mathbf{I} + \mu \left( \nabla \mathbf{v} + \nabla \mathbf{v}^T \right) \tag{1}$$

where v and p are the absolute velocity and the pressure, respectively,  $\mu$  is the fluid dynamic viscosity, and I is the identity tensor.

# 2.1 Navier-Stokes equations in an inertial frame

The fluid flow on a domain  $\Omega_f$  is governed by the Navier–Stokes equations, which on an inertial reference frame, are given by

$$\rho(\mathbf{v} \cdot \nabla)\mathbf{v} = -\nabla p + \mu \nabla^2 \mathbf{v} \quad \text{in } \Omega_f$$

$$\nabla \cdot \mathbf{v} = 0 \quad \text{in } \Omega_f$$
(2)

where  $\rho$  is the fluid density. A fluid flow problem involves Eq. 2 and boundary conditions for velocity or pressure. Velocity boundary conditions are imposed as Dirichlet boundary conditions, whilst pressure boundary conditions are imposed as normal stress conditions at the boundary  $\Gamma_P$  such as follows

$$\sigma n = -p_P n \quad \text{in } \Gamma_P \tag{3}$$

where n is the normal vector, and  $p_P$  is a prescribed pressure at the boundaries. Equation 3 imposes a normal stress condition and a no-tangential-stress condition.

# 2.2 Navier–Stokes equations in a rotating reference frame

When the reference frame is rotating at a constant angular velocity  $\omega$ , the observed velocity u is a relative velocity that can be related to the absolute velocity as follows

$$v = u + \omega \times s$$

where  $s = (r, \theta, z)$  is the position vector. When considering axisymmetry, the Navier–Stokes equations in terms of

(4)

relative velocities are obtained by the substitution of Eq. 4 in Eq. 2, and no coordinate transformation is required. The substitution gives rise to two extra terms in the Navier–Stokes equations: the Coriolis force and the centrifugal force. The resulting system of equations is given by

$$\rho(\boldsymbol{u}\cdot\nabla)\boldsymbol{u} = -\nabla p + \mu\nabla^2\boldsymbol{u} - \underbrace{2\rho\left(\boldsymbol{\omega}\times\boldsymbol{u}\right)}_{\text{Coriolis force}} - \underbrace{\rho\left(\boldsymbol{\omega}\times\boldsymbol{s}\right)}_{\text{centrifugal force}} \quad \text{in } \Omega_f$$

$$\nabla \cdot \boldsymbol{u} = 0 \qquad \qquad \text{in } \Omega_f$$
(5)

In this work, the rotation is around the z-axis, so  $\omega = (0, 0, \omega)$ . Also, axisymmetry conditions are considered, so the analysis is performed on  $\theta = 0$  and s = (r, 0, z).

#### 2.3 Material model

For topology optimisation, it is necessary to solve the equilibrium equations in an extended domain  $\Omega$  circumventing both the fluid  $(\Omega_f)$  and solid  $(\Omega_s)$  domains:  $\Omega = \Omega_s \cup \Omega_f$ . In Borrvall and Petersson (2003), the authors proposed modelling solid regions as porous material with low permeability. The permeability is described by an additional term in the Navier–Stokes equations known as the Darcy term. By considering the design variable field  $\alpha$  and a function  $\kappa$  that models the permeability as a function of design variables, the Navier–Stokes equations in an inertial reference frame (Eq. 2) with a Darcy term are given by

$$\rho(\mathbf{v} \cdot \nabla)\mathbf{v} + \nabla p - \mu \nabla^2 \mathbf{v} + \underbrace{\kappa(\alpha)(\mathbf{v} - \mathbf{v}_{\text{por}})}_{\text{Darcy term}} = 0 \quad \text{in } \Omega$$

$$\nabla \cdot \mathbf{v} = 0 \quad \text{in } \Omega$$

where  $v_{por}$  is the absolute velocity of the porous material (Alonso et al. 2018). For a rotating reference frame and a relative velocity  $u_{por}$  of the porous material, the Navier–Stokes equations with a Darcy term are

$$\rho(\mathbf{u} \cdot \nabla)\mathbf{u} + \nabla p - \mu \nabla^2 \mathbf{u} + 2\rho (\boldsymbol{\omega} \times \mathbf{u}) + \rho \boldsymbol{\omega} \times (\boldsymbol{\omega} \times \mathbf{s}) + \underbrace{\kappa(\alpha)(\mathbf{u} - \mathbf{u}_{\text{por}})}_{\text{Darcy term}} = 0 \quad \text{in } \Omega$$

$$\nabla \cdot \boldsymbol{u} = 0 \qquad \qquad \text{in } \Omega$$

In Eqs. 6 and 7, only one velocity expression can be assigned to all solid elements of the design domain. However, when optimising flow machines, it may be interesting to distinguish rotating parts from fixed parts. Hence, this work proposes a method that distinguishes solid at rest (stator) and rotating solid (rotor). The optimisation starts from an initial guess, the optimiser distributes stator and rotor elements in a 2D axisymmetric domain, and the 3D representation is obtained by rotating the 2D axisymmetric domain around the



**142** Page 4 of 23 E. Moscatelli et al.

shaft as illustrated by Fig. 2. The idea is to use two design variable fields  $\alpha$  and  $\beta$ , and to map the design variables into element phases according to Table 1.

The combination of two binary design variables provides four possible phases, but this work is interested in only three phases. By considering the combination  $\alpha=1$  and  $\beta=1$  as an undesired phase, the number of phases is reduced to three and the conditions  $\alpha=1$  and  $\beta=1$  are mutually exclusive. These mutually exclusive conditions enable adding linear terms to the governing equations that are active in only one part of the domain.

For the inertial reference frame, the absolute velocity of the stator is zero and the absolute velocity of the rotor is  $\omega r e_{\theta}$  in which  $e_{\theta}$  is the unit vector in  $\theta$  direction. Therefore, this work proposes extending the Navier–Stokes equations to the stator and rotor phases as follows

$$\begin{split} \rho(\mathbf{v}\cdot\nabla)\mathbf{v} + \nabla p - \mu\nabla^2\mathbf{v} + \kappa(\alpha)\mathbf{v} + \kappa(\beta)(\mathbf{v} - \omega \, r\, \boldsymbol{e}_\theta) &= 0 &\quad \text{in } \Omega \\ \nabla\cdot\mathbf{v} &= 0 &\quad \text{in } \Omega \end{split}$$

For the rotating reference frame, the relative velocity of the rotor is zero and the relative velocity of the stator is  $-\omega r e_{\theta}$ . Therefore, the proposed extension to the stator and rotor phases is given by

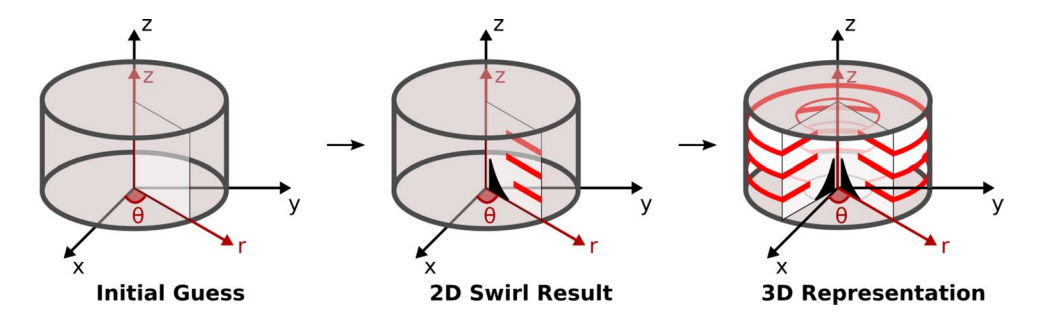
$$\begin{split} \rho(\boldsymbol{u}\cdot\nabla)\boldsymbol{u} + \nabla p - \mu \nabla^2 \boldsymbol{u} + 2\rho\left(\boldsymbol{\omega}\times\boldsymbol{u}\right) + \rho\,\boldsymbol{\omega}\times\left(\boldsymbol{\omega}\times\boldsymbol{s}\right) \\ + \kappa(\alpha)(\boldsymbol{u} + \omega\,r\,\boldsymbol{e}_{\theta}) + \kappa(\beta)\boldsymbol{u} &= 0 & \text{in } \Omega \\ \nabla\cdot\boldsymbol{u} &= 0 & \text{in } \Omega \end{split}$$

According to Table 1 and Eqs. 8 and 9, it is necessary that the interpolation function  $\kappa$  maps an input of 1 to  $\kappa_{\text{max}}$  and a input of 0 to  $\kappa_{\text{min}}$ . By considering  $\kappa_{\text{min}} = 0$  and recalling that it is possible to consider a linear material model with

**Table 1** Proposed mapping between design variables and element phases

α	β	Element phase
1	0	Stator (solid)
0	0	Fluid
0	1	Rotor (solid)
1	1	Undesired phase

**Fig. 2** Illustration of the proposed method to design a rotor-stator device



the discrete design variable approach to fluid flow problems (Souza et al. 2021), the selected function  $\kappa$  is

$$\kappa(\alpha) = \kappa_{\text{max}} \alpha$$

$$\kappa(\beta) = \kappa_{\text{max}} \beta$$
(10)

The maximum inverse permeability may be calculated from the Darcy number (Da) and the dynamic viscosity. The Darcy number is defined as follows

$$Da = \frac{\mu}{\kappa_{\text{max}} L_c^2} \tag{11}$$

where  $L_c$  is a characteristic length. In this work, the characteristic length is considered to be the inlet size. The Reynolds number is calculated based on the characteristic velocity  $V_c$  as follows

$$Re = \frac{\rho V_c L_c}{\mu}$$
 (12)

where the characteristic velocity may be, for example, the maximum velocity magnitude in the domain or the maximum inlet velocity in the axial direction.

# 2.4 Optimisation algorithm

The use of Eqs. 8 and 9 for topology optimisation require that the undesired phase  $\alpha=1$  and  $\beta=1$  (Table 1) is not reached by any element. In this work, we propose a modification to the TOBS algorithm that avoids the undesired phase. Before presenting this modification, it is useful to present the TOBS algorithm as proposed by Sivapuram and Picelli (2018) to emphasize where the modification is made. The general topology optimisation problem can be expressed mathematically as

$$\min_{\alpha} F(\mathbf{w}(\alpha), \alpha) = F(\alpha)$$
s.t.  $G_i(\mathbf{w}(\alpha), \alpha) \le \overline{G}_i, \quad i = 1, ..., M$ 

$$\alpha(\mathbf{x}) \in \{0, 1\}, \quad \forall \mathbf{x} \in \Omega$$
(13)

where F is the objective function, w is the vector of state variables,  $\alpha$  is the design variable field,  $G_i$  are the constraints,



$$\alpha^{k+1} = \alpha^k + \Delta \alpha^k \tag{14}$$

By considering the expansion of the objective function by the Taylor series as follows

$$F(\alpha + \Delta \alpha) = F(\alpha) + \frac{\partial F}{\partial \alpha} \Delta \alpha + \mathcal{O}(\Delta \alpha^2)$$
 (15)

and noticing that, as  $F(\alpha^k)$  is constant (because  $\alpha^k$  is already known), the minimization of  $F(\alpha + \Delta \alpha)$  is approximately the minimization of  $\frac{\partial F}{\partial \alpha} \Delta \alpha$ . By also considering the linearization of the constraints  $G_i$ , the linearized optimisation problem may be written as

$$\begin{aligned} & \min_{\Delta\alpha} \frac{\partial F}{\partial \alpha_j} \Delta \alpha_j \\ & \text{s.t.} \frac{\partial G_i}{\partial \alpha_j} \Delta \alpha_j \leq \overline{G}_i - G_i(\alpha^k) = \Delta G_i, \quad i = 1, \dots, M \\ & ||\Delta\alpha||_1 \leq \zeta N \\ & \Delta\alpha_j \in \{0, +1\} \text{ if } \alpha_j = 0, \quad j = 1, \dots, N \\ & \Delta\alpha_j \in \{-1, 0\} \text{ if } \alpha_j = 1, \quad j = 1, \dots, N \end{aligned}$$

where  $\zeta$  is a small parameter to limit the number of design variable changes and to keep the linearization error small. Also, it is necessary to relax the constraints to limit  $\Delta G_i$  and to avoid infeasible integer sub-problems. The constraints are relaxed by small parameters  $\epsilon_i$  according to the following equation

$$\Delta G_{i} = \begin{cases} -\epsilon_{i} G_{i}(\alpha^{k}), & \overline{G}_{i} < (1 - \epsilon_{i}) G_{i}(\alpha^{k}) \\ \overline{G}_{i} - G_{i}(\alpha^{k}), & \overline{G}_{i} \in \left[ (1 - \epsilon_{i}) G_{i}(\alpha^{k}), (1 + \epsilon_{i}) G_{i}(\alpha^{k}) \right] \\ \epsilon_{i} G_{i}(\alpha^{k}), & \overline{G}_{i} > (1 + \epsilon_{i}) G_{i}(\alpha^{k}) \end{cases}$$

$$(17)$$

In the TOBS approach, the original design variable field  $\alpha$  is kept discrete by controlling the step  $\Delta\alpha_j$  of each design variable  $\alpha_j$  with the bound constraints as shown in Eq. 16. In this work, a similar approach is used to avoid the undesired state  $\alpha_j = 1$  and  $\beta_j = 1$ . First, the bound constraints are computed from the proper selection of the sets  $S_{\alpha_j}$  and  $S_{\beta_j}$ . Then, extra constraints  $H_j(\Delta\alpha_j, \Delta\beta_j)$  are added for each element to avoid transitions to the undesired state. The resulting optimisation problem is presented in Eq. 18 and the values of  $S_{\alpha_j}$ ,  $S_{\beta_j}$ ,  $H_j$  are presented in Table 2.

$$\min_{\Delta\alpha,\,\Delta\beta} \frac{\partial F}{\partial \alpha_{j}} \Delta\alpha_{j} + \frac{\partial F}{\partial \beta_{j}} \Delta\beta_{j}$$
s.t. 
$$\frac{\partial G_{i}}{\partial \alpha_{j}} \Delta\alpha_{j} + \frac{\partial G_{i}}{\partial \beta_{j}} \Delta\beta_{j} \leq \Delta G_{i}, \quad i = 1, ..., M$$

$$H_{j}(\Delta\alpha_{j},\,\Delta\beta_{j}) \leq 0, \quad j = 1, ..., N$$

$$||\Delta\alpha||_{1} \leq \zeta N$$

$$||\Delta\beta||_{1} \leq \zeta N$$

$$\Delta\alpha_{j} \in S_{\alpha_{j}}, \quad j = 1, ..., N$$

$$\Delta\beta_{i} \in S_{\beta_{i}}, \quad j = 1, ..., N$$
(18)

The addition of linear constraints  $H_j$  increases the computational cost of each call to the integer linear optimisation algorithm. However, the additional cost is not prohibitive as it is shown in Sect. 4.1.2.

# 2.5 Case problems

#### 2.5.1 Tesla pump

The selected problem to show the proposed algorithm in a rotating reference frame is the design of a Tesla pump: a centrifugal bladeless pump in which the pumping effect is obtained by the boundary layer and Coandă effects. The novelty of the results presented in this work is the simultaneous design of the rotor and the stator. The approach considered here is different from other works that focused the optimisation on the rotor (Alonso et al. 2019).

In this work, the Tesla pump optimisation considers the pump efficiency  $\eta$  and the pressure head H. The pump efficiency  $\eta$  is the ratio of the power added to the fluid  $(P_f)$  by the power used to drive the pump (Okubo et al. 2021). The pump efficiency can be calculated as follows

$$\eta = \frac{P_f}{T \cdot \omega} \tag{19}$$

**Table 2** Bound constraints  $(S_{\alpha_j} \text{ and } S_{\beta_j})$  and extra constraints  $(H_j)$  for the proposed optimisation problem

$\alpha_j$	$\beta_{j}$	Element phase	$S_{lpha_j}$	$S_{oldsymbol{eta}_j}$	$H_j$
1	0	Stator (solid)	{-1,0}	{0, 1}	$\Delta \alpha_j + \Delta \beta_j$
0	0	Fluid	$\{0, 1\}$	$\{0, 1\}$	$\Delta \alpha_j + \Delta \beta_j - 1$
0	1	Rotor (solid)	$\{0, 1\}$	$\{-1,0\}$	$\Delta \alpha_i + \Delta \beta_i$
1	1	Undesired phase	-	_	-

where

$$P_f = \int_{\Gamma} \left( p + \rho \frac{\mathbf{v} \cdot \mathbf{v}}{2} \right) (\mathbf{v} \cdot \mathbf{n}) \, 2\pi r \, \mathrm{d}\Gamma \tag{20}$$



$$T = \int_{\Gamma} \rho(s \times v)(v \cdot n) \, 2\pi r \, d\Gamma \tag{21}$$

The maximization of the pump efficiency is related to the minimization of the pump power dissipation. According to Okubo et al. (2021), the minimization of the pump power dissipation is equivalent to the minimization of the following functional

$$J(\boldsymbol{u}, p) = -\int_{\Gamma} \left(\frac{p}{\rho} + \frac{\boldsymbol{u} \cdot \boldsymbol{u}}{2}\right) (\boldsymbol{u} \cdot \boldsymbol{n}) \, 2\pi r \, d\Gamma$$
 (22)

and by applying the divergence theorem it is possible to obtain a definition of the same functional over the domain instead of the boundary as follows

$$J(\boldsymbol{u}, p) = -\int_{\Omega} \boldsymbol{u} \cdot \left(\frac{\nabla p}{\rho} + (\boldsymbol{u} \cdot \nabla)\boldsymbol{u}\right) 2\pi r \,\mathrm{d}\Omega \tag{23}$$

The pressure head is the energy supplied to the fluid in length units. The pressure head can be calculated as follows

$$H = \frac{1}{\dot{V}} \int_{\Gamma} \left( \frac{p}{\rho g} + \frac{\mathbf{v} \cdot \mathbf{v}}{2 g} \right) (\mathbf{v} \cdot \mathbf{n}) \ 2\pi r \, \mathrm{d}\Gamma$$
 (24)

where  $\dot{V}$  is the flow rate across the pump and g is the gravitational acceleration. The maximization of the pressure head is related to the minimization of the relative energy dissipation  $\Phi_R$  (Alonso et al. 2019). The relative energy dissipation is calculated by the following equation

$$\Phi_R(\mathbf{u}) = Ed_R(\mathbf{u}) + Po_R(\mathbf{u}) + In_R(\mathbf{u})$$
(25)

where  $Ed_R(\mathbf{u})$  is the relative viscous energy dissipation functional,  $Po_A(\mathbf{u})$  is the porosity functional, and  $In_R(\mathbf{u})$  is the inertial forces functional. They are calculated as follows

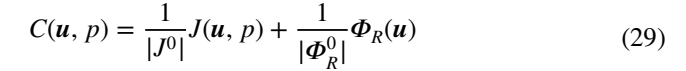
$$Ed_{R}(\boldsymbol{u}) = \frac{\mu}{2} \int_{\Omega} (\nabla \boldsymbol{u} + \nabla \boldsymbol{u}^{T}) : (\nabla \boldsymbol{u} + \nabla \boldsymbol{u}^{T}) 2\pi r \, d\Omega \qquad (26)$$

$$Po_{R}(\mathbf{u}) = \int_{\Omega} \kappa(\alpha)(\mathbf{u} + \omega r \mathbf{e}_{\theta}) \cdot (\mathbf{u} + \omega r \mathbf{e}_{\theta}) 2\pi r d\Omega$$
$$+ \int_{\Omega} \kappa(\beta) \mathbf{u} \cdot \mathbf{u} 2\pi r d\Omega$$
(27)

$$In_{R}(\mathbf{u}) = \int_{\Omega} 2\rho \left(\boldsymbol{\omega} \times \mathbf{u}\right) \cdot \mathbf{u} \, 2\pi r \mathrm{d}\Omega$$

$$+ \int_{\Omega} \left[\rho \, \boldsymbol{\omega} \times (\boldsymbol{\omega} \times \boldsymbol{s})\right] \cdot \mathbf{u} \, 2\pi r \, \mathrm{d}\Omega$$
(28)

Then, the Tesla pump design is performed by the minimization of the following objective function, taking both effects into account



where  $J^0$  and  $\Phi_R^0$  are the functional J and relative energy dissipation calculated for the initial guess.

#### 2.5.2 Labyrinth seal

The selected problem to present the proposed algorithm in a fixed reference frame is the design of a labyrinth seal. Labyrinth seals are non-contacting seals that reduce leakage by offering a tortuous path to the fluid flow. They are mounted between the rotor and stator of flow machines, so it is necessary to include the velocity differences between the rotor and stator for modelling the flow inside a labyrinth seal. Therefore, from this context, the topology optimisation algorithm proposed in this work may design the rotating and stationary parts of the labyrinth seals simultaneously.

The objective function to be minimized for the labyrinth seal case is the leakage through the outlet surface  $\Gamma_{\rm out}$ , which is given by

$$Q(\mathbf{v}) = \int_{\Gamma_{\text{out}}} \rho(\mathbf{v} \cdot \mathbf{n}) \, 2\pi r \, \mathrm{d}\Gamma \tag{30}$$

However, the minimization of the leakage in a channel is achieved by constricting the fluid flow path, so it is necessary to guarantee a minimum gap between the rotor and the stator to avoid closing the flow passage when minimizing the leakage.

# 2.6 Minimum gap between rotor and stator

The minimization of leakage is used for the topology optimisation of a labyrinth seal. However, the optimised design that may be obtained for minimum leakage is a closed fluid channel, which is not feasible for the labyrinth seal because the stator and rotor have different velocities. Therefore, it is necessary to modify the problem formulation to avoid closing the channel. The solution adopted in this work is to impose a minimum distance (gap) between the rotor and the stator. The problem of maintaining a gap between two phases has been solved in literature by works based on continuous design variables. For example, in the context of heat exchangers design, Kobayashi et al. (2021) define the elements with intermediate values of the design variable as solid and the elements with minimum and maximum values as two different fluids. Høghøj et al. (2020) use filtering and projection for maintaining a solid gap between two different fluids. These approaches may also work for maintaining a fluid gap between solid at different velocities. However, in this work, discrete design variables are used, so there are no intermediate values and filtering the design variables



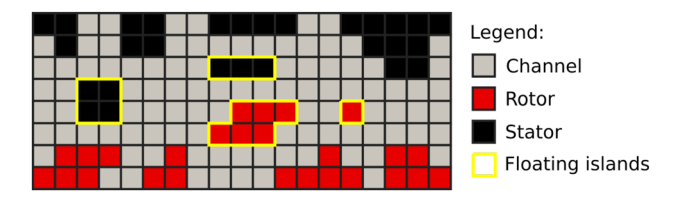


Fig. 3 Illustration of floating islands of solid material (highlighted with yellow frames) during the topology optimisation of rotor-stator devices. (colour figure online)

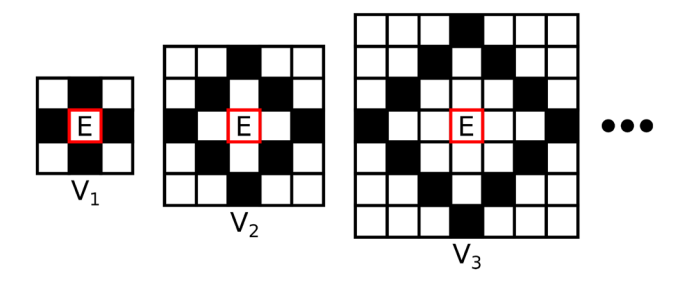


Fig. 4 Schematic representation of the neighbourhoods  $V_R$  of element E for R = 1, 2, 3

would reintroduce greyscale. Therefore, a new approach is

Another feature that may be undesired in labyrinth seal design is the possible formation of floating islands of solid material during topology optimisation (Fig. 3) because they may be hard to manufacture and assemble. Also, the manufacturing process would require introducing additional structures, such as some circumferentially spaced arms. Therefore, in this work, the formation of floating islands in the topology optimisation of the labyrinth seal is disallowed.

The method used to impose a minimum gap between rotor and stator and to avoid the arising of floating solid islands is to control the allowed changes of the design variables. This is done by defining neighbourhoods  $V_R$  of each element where R is the  $\ell_1$  distance between the element and the elements in  $V_R$ . Figure 4 presents a graphical representation of the neighbourhoods  $V_R$ .

The solid islands are avoided by allowing only the following phase changes: (1) fluid elements close to rotor can change to rotor; (2) fluid elements close to stator can change to stator; (3) stator elements close to fluid can change to fluid; (4) rotor elements close to fluid can change to fluid. An illustration of the allowed changes for labyrinth seal design is presented in Fig. 5 where the elements that are allowed to change are marked with numbers.

The allowed changes described in Fig. 5 require the definition of the phases in the boundary. This can be done by extending the domain on all sides by one element and by defining the phases of the introduced elements. Figure 6

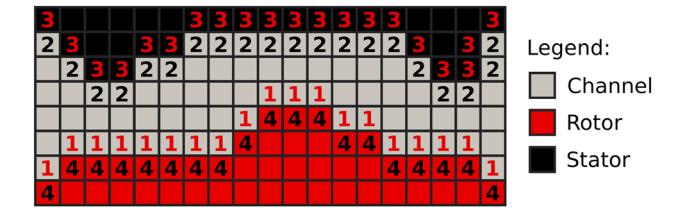


Fig. 5 Illustration of active elements during the optimisation of a labyrinth seal. (1) Fluid elements that can change to rotor; (2) fluid elements that can change to stator; (3) stator elements that can change to fluid; (4) rotor elements that can change to fluid. Elements with black numbers are active during stator expansion/rotor contraction and elements with red numbers are active during rotor expansion/stator contraction. (colour figure online)

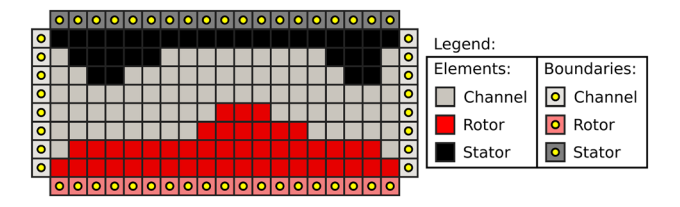


Fig. 6 Example of a possible boundary initialization for the labyrinth seal problem

presents an example of initialization for the boundaries. It is important to notice that the extended boundary elements are not part of the analysis and optimisation. They are only used to complete the  $V_1$  neighbourhood of elements at the border of the domain.

However, it is still possible to obtain solid islands if all elements of the design domain are allowed to change in each call to the integer linear optimisation routine because adjacent elements can change simultaneously as Fig. 7 shows. As the logic to determine the allowed changes is based on the current state (i.e., there is no information about the next state), it is necessary to break the iteration into two steps to avoid adjacent elements of different phases changing at the same time. Therefore, each iteration of the labyrinth seal design is divided into two steps: stator expansion/rotor contraction and stator contraction/rotor expansion. During stator expansion/rotor contraction, fluid elements close to stator and rotor elements close to fluid elements are allowed to change. This corresponds to the black numbers in Fig. 5. During stator contraction/rotor expansion, fluid elements close to rotor elements are allowed to change to rotor and stator elements close to fluid elements are allowed to change to fluid. This corresponds to red numbers in Fig. 5.

It is possible to impose a minimum gap (distance) between the rotor and stator  $g_{\min}$  by considering the neighbourhood  $V_R$  with R given by



**142** Page 8 of 23 E. Moscatelli et al.

$$R = \operatorname{ceil}\left(\frac{g_{\min}}{h}\right) \tag{31}$$

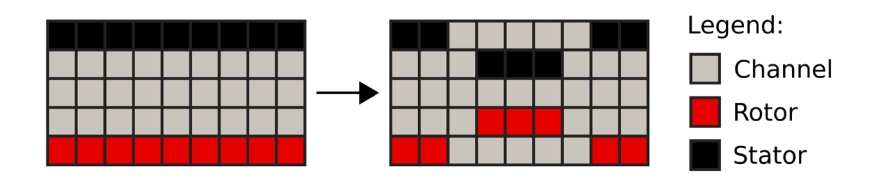
where h is the element size and the ceil function returns the least integer that is greater than the argument. Then, the neighbourhoods  $V_1$  and  $V_R$  are used to define the allowed changes of each element. If an element E is in stator phase, it is allowed to change to fluid phase if there is a fluid element in  $V_1(E)$ . Otherwise, the element E must remain in stator phase. Similarly, if an element E is in rotor phase, it

is allowed to change to fluid phase if there is a fluid element in  $V_1(E)$ . Otherwise, the element E must remain in rotor phase. For a fluid element E there are two possibilities for change. If there is a stator element in  $V_1(E)$  and there is **no** rotor element in  $V_R(E)$ , the element is allowed to change to stator. Else, if there is a rotor element in  $V_1(E)$  and there is **no** stator element in  $V_R(E)$ , the element is allowed to change to rotor. Otherwise, the element must remain in fluid phase. This algorithm is described in pseudocode by Algorithm 1.

Algorithm 1 Algorithm to identify the allowed changes to each element of the optimisation of labyrinth seal.

```
1: procedure LabsealAllowedChanges
 2:
          if E is STATOR: then
               if FLUID in V_1(E): then
 3:
                    S_{\alpha_E} \leftarrow \{0\}
 4:
                    S_{\beta_E} \leftarrow \{-1, 0\}
 5:
 6:
                    S_{\alpha_E} \leftarrow \{0\}
 7:
                    S_{\beta_E} \leftarrow \{0\}
 8:
          else if E is ROTOR: then
 9:
               if FLUID in V_1(E): then
10:
                    S_{\alpha_E} \leftarrow \{-1, 0\}
11:
                    S_{\beta_E} \leftarrow \{0\}
12:
13:
14:
                    S_{\alpha_E} \leftarrow \{0\}
15:
                    S_{\beta_E} \leftarrow \{0\}
          else if E is FLUID: then
16:
               if STATOR in V_1(E) and not ROTOR in V_R(E): then
17.
                    S_{\alpha_E} \leftarrow \{0\}
18:
                    S_{\beta_E} \leftarrow \{0, 1\}
19:
               else if ROTOR in V_1(E) and not STATOR in V_R(E): then
20:
21:
                    S_{\alpha_E} \leftarrow \{0, 1\}
                    S_{\beta_E} \leftarrow \{0\}
22:
23:
                    S_{\alpha_E} \leftarrow \{0\}
24:
                    S_{\beta_E} \leftarrow \{0\}
25:
```

Fig. 7 Arise of floating islands of solid material when running the optimisation of labyrinth seal with just one call to the integer linear optimisation algorithm by iteration





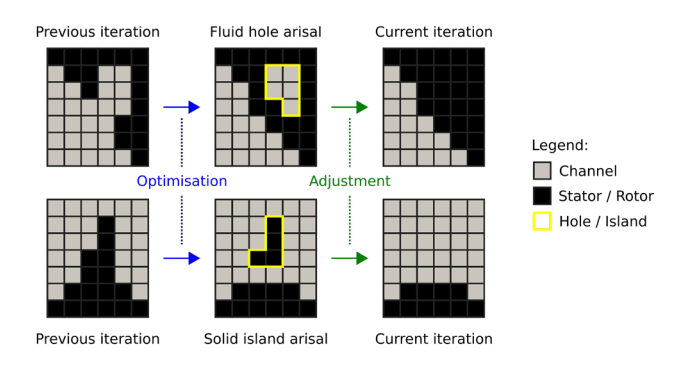


Fig. 8 Example of solid floating islands and fluid holes arisal and removal during optimisation

The Algorithm 1 may still produce solid floating islands if solid elements (rotor or stator) that connect other solid elements to the walls are removed as illustrated by Fig. 8. Similarly, a fluid hole may be created when two solid parts are merged. Although fluid holes are not problematic for labyrinth seal operation, they may facilitate the arisal of solid floating islands. Also, there is no fluid flow inside fluid holes, so filling the hole does not affect the objective function. Therefore, an adjustment is performed after each call to the optimisation routine to remove solid floating islands and fluid holes of the design as described by Fig. 8.

The Algorithm 1 guarantees proper changes in design variables, i.e., the undesired state  $\alpha_{\rm E}=1$  and  $\beta_{\rm E}=1$  is avoided. Therefore, the constraints  $H_j$  presented in Table 2 are not necessary when using the minimum gap modification. This reduces the cost of each call to the integer linear programming optimisation algorithm. However, the modification for guaranteeing the minimum gap reduces the optimiser freedom in changing the design topology and it may be not interesting for some problems, such as the Tesla pump problem. So, the minimum gap modification is used just for the labyrinth seal problem in this work.

# 3 Numerical implementation

The proposed algorithm follows the common steps taken by topology optimisation methods such as the TOBS approach (Sivapuram and Picelli 2018): to start from an initial guess and to iterate the solution of the forward problem (governing equations), the sensitivity analysis, and the mathematical programming problem until convergence is reached. A flowchart illustrating the proposed topology optimisation algorithm is presented in Fig. 9.

The governing equations are solved using the Finite Element Method (FEM) through the FEniCS platform Alnæs et al. (2015). The Navier–Stokes equations are solved fully coupled using an implementation of the Newton–Raphson method from PETSc (Balay et al. 2021a, b). The sensitivity

analysis is performed by following the discrete adjoint approach and automatic differentiation from the dolfinadjoint library (Farrell et al. 2013; Mitusch et al. 2019). The optimisation algorithm is solved with the default integer linear optimisation routine of CPLEX® from IBM®, which implements a branch-and-bound algorithm. The considered optimisation stop criteria are a maximum number of iterations  $n_{\rm max}$  and a verification for loops in the design variable. At each iteration, the design variables are compared to the design variables of the last  $n_{\rm loop}$  iterations. If the current iteration has the same design variables of any of the last  $n_{\rm loop}$  iterations, the optimisation has entered a loop and the optimisation can be stopped.

The Tesla pump optimisation results are post-processed by filling fluid regions that do not contribute to the objective function with the surrounding solid phase (rotor or stator). The post-processing algorithm consists of selecting thresholds  $\overline{J}$  and  $\overline{\Phi}_R$  for J and  $\Phi_R$ , respectively, and by replacing the fluid elements that present specific values of |J| and  $|\Phi_R|$  lower than  $\overline{J}$  and  $\overline{\Phi}_R$  with rotor or stator elements if there is a rotor or stator element in the neighbourhood  $V_1$  of the fluid element. This replacement process is successively repeated until there are no more changes of phase. The thresholds are selected as follows

$$k_{J} = \begin{cases} \log_{10} (1 + |J|) & |J| \ge 1\\ \log_{10} \left( 1 + \frac{1}{|J|} \right) & |J| < 1 \end{cases}$$
 (32)

$$\overline{J} = 10^{k_J - k} \tag{33}$$

where k is an arbitrary parameter calibrated to avoid changing the objective function values  $(C, J, \text{ and } \Phi_R)$ . The same procedure is used to obtain  $\overline{\Phi}_R$ . In this work, the parameter k = 6 is used.

#### 4 Results

This section presents results obtained by applying the proposed method to two design problems: a Tesla pump and a labyrinth seal.

#### 4.1 Tesla pump

The Tesla pump considered in this work has a central rotating shaft, the fluid enters parallel to the shaft, and leaves the pump radially according to Fig. 10. As the pump is axisymmetric, it can be modelled in a 2D mesh using cylindrical coordinates and axisymmetry in the off-plane direction  $\theta$ . Also, the selected reference frame is rotating with the shaft.



**142** Page 10 of 23 E. Moscatelli et al.

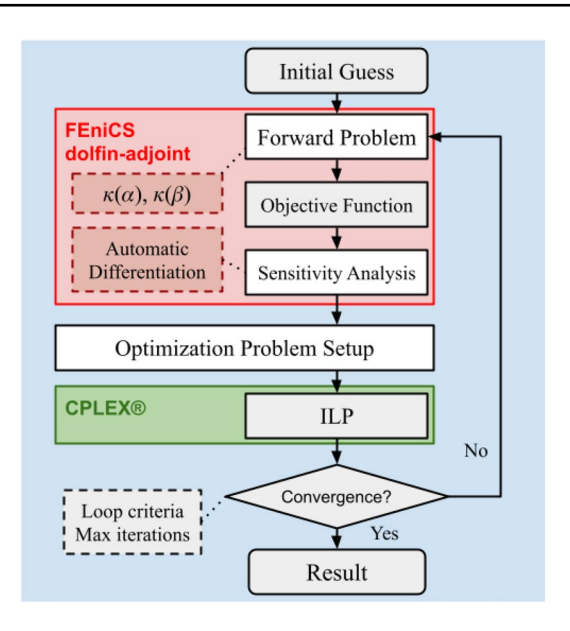


Fig. 9 Flowchart illustrating the topology optimisation procedure used in this work

The fluid properties used for simulation are  $\mu=0.0146$  Pa.s and  $\rho=835.2$  kg/m³ which correspond to oil SAE 15W-40. The diameter of the shaft is D=5.2 mm, the height and width of the design domain are L=10 mm and H=12.4 mm, respectively, the inlet size  $e_H$  is 2.4 mm, and the angular velocity  $\omega$  is 400 rpm (unless otherwise noted). The inlet velocity has a parabolic profile in the axial and tangential directions, and is zero in the radial direction. The maximum axial velocity in inlet is  $V_c=0.36$  m/s (Re = 50) at the centre of the inlet. The inlet velocity profile in the tangential direction is half of a parabola with the maximum value of  $-\omega$  ( $D/2+e_H$ ) close to the stator wall. The Darcy number is Da =  $10^{-6}$ . The optimisation parameters are a truncation error parameter of  $\zeta=0.1\%$ , a maximum number of iterations

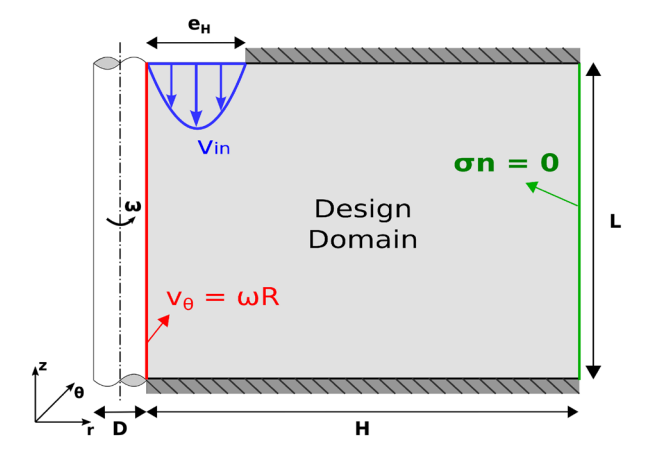


Fig. 10 Tesla pump design domain and boundary conditions



 $n_{\rm max}=1000$ , and loop convergence criteria  $n_{\rm loop}=50$ . The element size is 0.1 mm, resulting in a structured mesh of  $124\times100$  quadrilateral elements for simulation and optimisation. The velocity, pressure, and design variable fields are discretized by quadratic, linear, and piece-wise polynomials, respectively.

The results presented in Fig. 11 are obtained by starting the optimisation from different initial guesses. The first initial guess contains only fluid elements (Fig. 11a). The other initial guesses are inspired by Tesla pump rotors composed of parallel rotor disks (Fig. 11d, g). Each row of Fig. 11 presents a different optimisation case with the initial guess in the first column, the result in the second column, and the post-processed result in the third column. The convergence graphs for the results of Fig. 11 are presented in Fig. 12.

The initial guess composed of only fluid elements has a negative pressure head, i.e., it does not work as a pump (Table 3). Therefore, the pump efficiency is not defined for Fig. 11a and the optimisation problem is not capable of designing a Tesla pump as observed in Fig. 11b and c. The same behaviour is observed when starting with one rotor disk, so the result is not presented. When starting with two disks (Fig. 11d), the initial configuration has a positive pressure head and the optimisation is successful in optimising the pump efficiency as observed in Table 3. In Table 3, the parameters with the "0" superscript indicate the value at the initial guess and the parameters with the "\*" superscript indicate the post-processed parameter. For the optimisation starting with only fluid elements (first row of Table 3), it is possible to observe that the pump efficiency has no physical sense (values greater than 100%).

For the optimisation starting with only fluid elements (Fig. 11a), the optimisation result has no rotor elements (Fig. 11b). The optimiser places the contour of the stator in the regions that impose fewer obstacles to flow. As the fluid enters the design domain axially at the upper-left part of the domain and leaves at the right edge, the region that imposes less obstacle to flow is the upper-right part of the domain. The optimisation reduces the objective function, but it is not able to generate a pumping configuration. The minimisation of relative energy dissipation dominates the optimisation when starting with only fluid elements.

For the case starting with two rotor disks (Fig. 11d), the topology optimisation algorithm modifies the starting disks to reduce the obstacle to the entering flow. The algorithm also introduces more disks to increase the efficiency (Fig. 11e). By the end of the optimisation, the pressure head and the viscous energy dissipation increase (Fig. 12b). The viscous effects are important for increasing the pressure head, but the viscous effects may also increase the viscous energy dissipation. Also, the efficiency increased because the energy transferred to the fluid increased more than the dissipated energy. For the initial guess with three

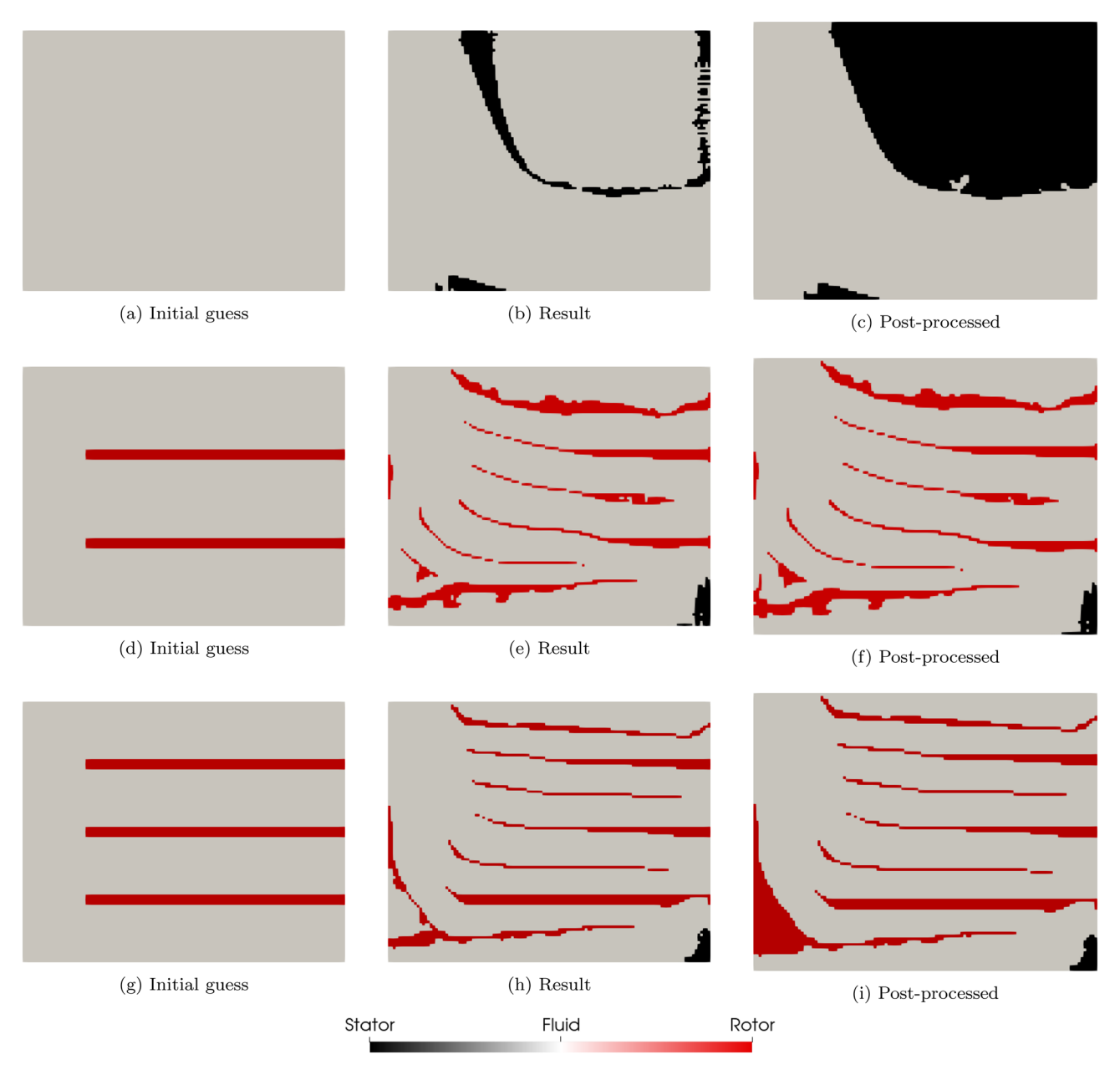


Fig. 11 Tesla pump optimisation results by starting the optimisation from different initial guesses. Each row presents an optimisation case. The first column indicates the initial guesses, the second column shows the results, and the third column presents the post-processed results

disks (Fig. 11g), the topology optimisation algorithm also introduces more rotor disks and the lower disk attached to the shaft is a single structure without floating solid islands (Fig. 11h). According to Table 3, the efficiency gain for the optimisation starting with two disks is greater.

The convergence graphs of Fig. 12 present the behaviour of the objective function (C), the pump power dissipation functional (J), the relative energy dissipation  $(\Phi_R)$ , and the pressure head (H) during the optimisation. The objective function and the pump power dissipation functional

decreased for all optimisation cases. The relative energy dissipation decreased for the optimisation starting with only fluid elements (Fig. 12a), because the minimization of energy dissipation dominated the optimisation as the pump efficiency is not well defined for negative pressure head. The relative energy dissipation increased in Fig. 12b and c because the viscous effects are important for pumping the fluid (i.e., for increasing the pressure head), but the viscous effects may also increase the viscous energy dissipation as discussed in the previous paragraph. During some iterations,



**142** Page 12 of 23 E. Moscatelli et al.

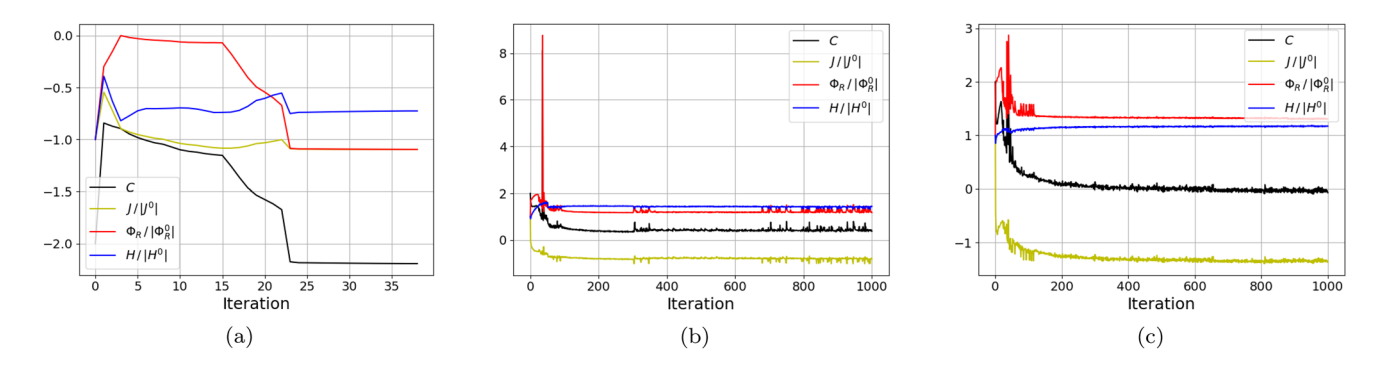


**Fig. 12** Convergence graphs for the Tesla pump optimisation cases of Fig. 11. The objective function (C) is presented in black, the scaled pump power dissipation  $(J/|J^0|)$  is presented in yellow, the scaled energy dissipation  $(\boldsymbol{\Phi}_R/|\boldsymbol{\Phi}_R^0|)$  is presented in red, and the scaled

pressure head  $(H/|H^0|)$  is presented in blue. a Convergence graph for the first row of Fig. 11, **b** Convergence graph for the second row of Fig. 11, and **c** Convergence graph for the third row of Fig. 11. (colour figure online)

**Table 3** Tesla pump performance parameters for the results of Fig. 11

Initial guess	$J^0$ [W/(kg/m <sup>3</sup> )]	$J^*$ [W/(kg/m <sup>3</sup> )]	$\Phi_R^0  (\mathrm{mW})$	${\bf \Phi}_R^*  ({\rm mW})$	$\eta^0$ (%)	η* (%)	$H^0$ (mm)	H* (mm)
0 Disks	- 2.02	- 2.18	- 1.5	- 1.7	495	336	- 5.0	- 3.8
2 Disks	1.06	-0.85	2.0	2.3	35	63	14.5	21.0
3 Disks	0.62	-0.84	2.3	3.0	46	65	19.8	23.2

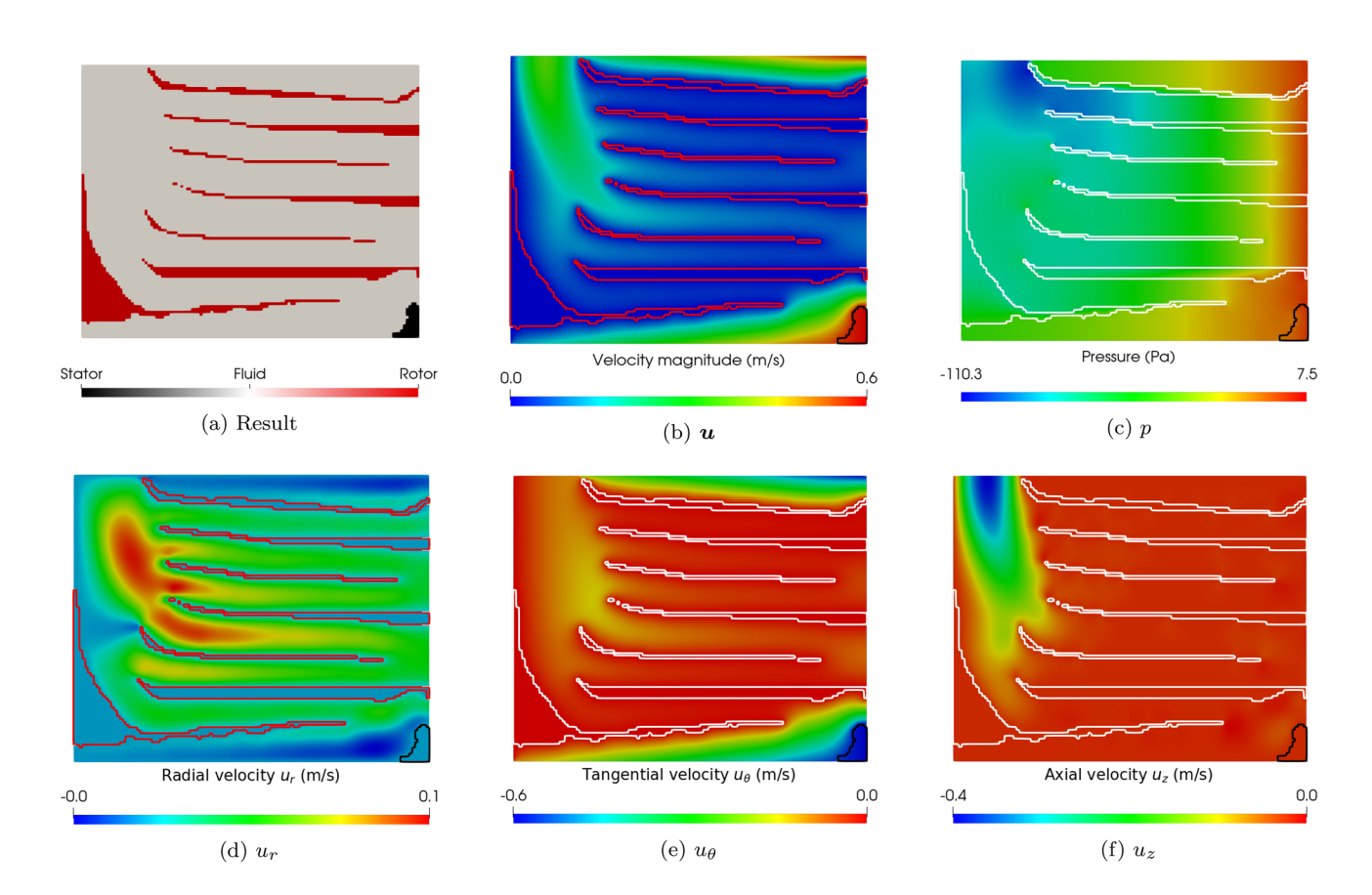
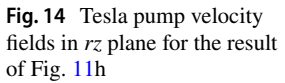


Fig. 13 Tesla pump optimisation result and flow fields by starting the optimisation with three rotor disk (Fig. 11g)





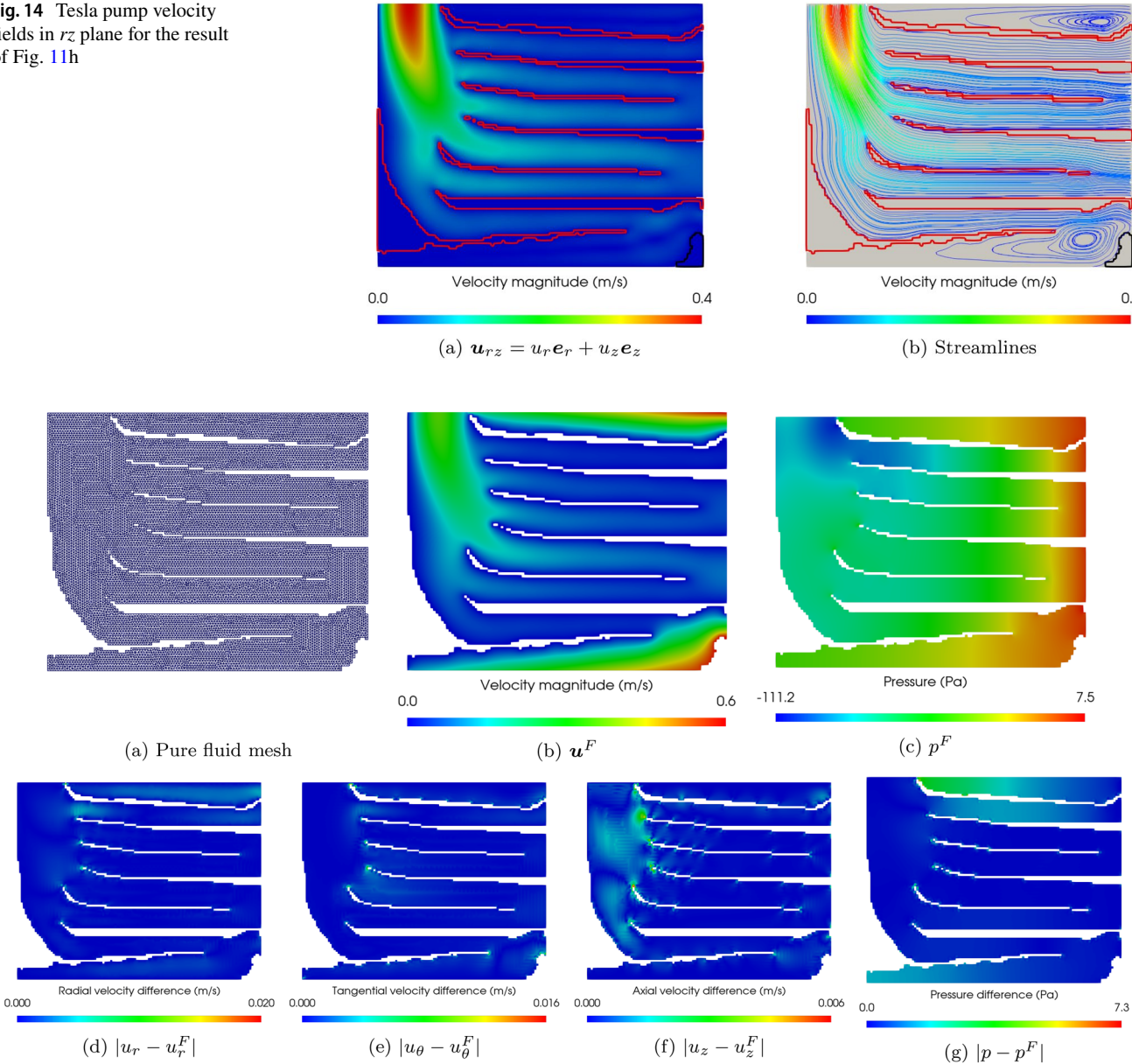


Fig. 15 Analysis of the Tesla pump topology optimisation result in a pure fluid domain. a Pure fluid mesh, b Velocity magnitude for the pure fluid mesh, c Pressure for the pure fluid mesh, d Radial veloc-

ity difference, e Tangential velocity difference, f Axial velocity difference, and g Pressure difference

Table 4 Comparison of the Tesla pump parameters obtained with a pure fluid domain with the parameters obtained in an extended domain with Darcy term for modelling solid phases

Domain	Equations	Figures	J [W/(kg/m <sup>3</sup> )]	$\Phi_R$ (mW)	η (%)	H (mm)
Extended	Equation 9	Figure 13	0.8427	3.0189	64.789	23.174
Pure fluid	Equation 5	Figure 15	0.8632	3.0130	64.842	22.947



**142** Page 14 of 23 E. Moscatelli et al.

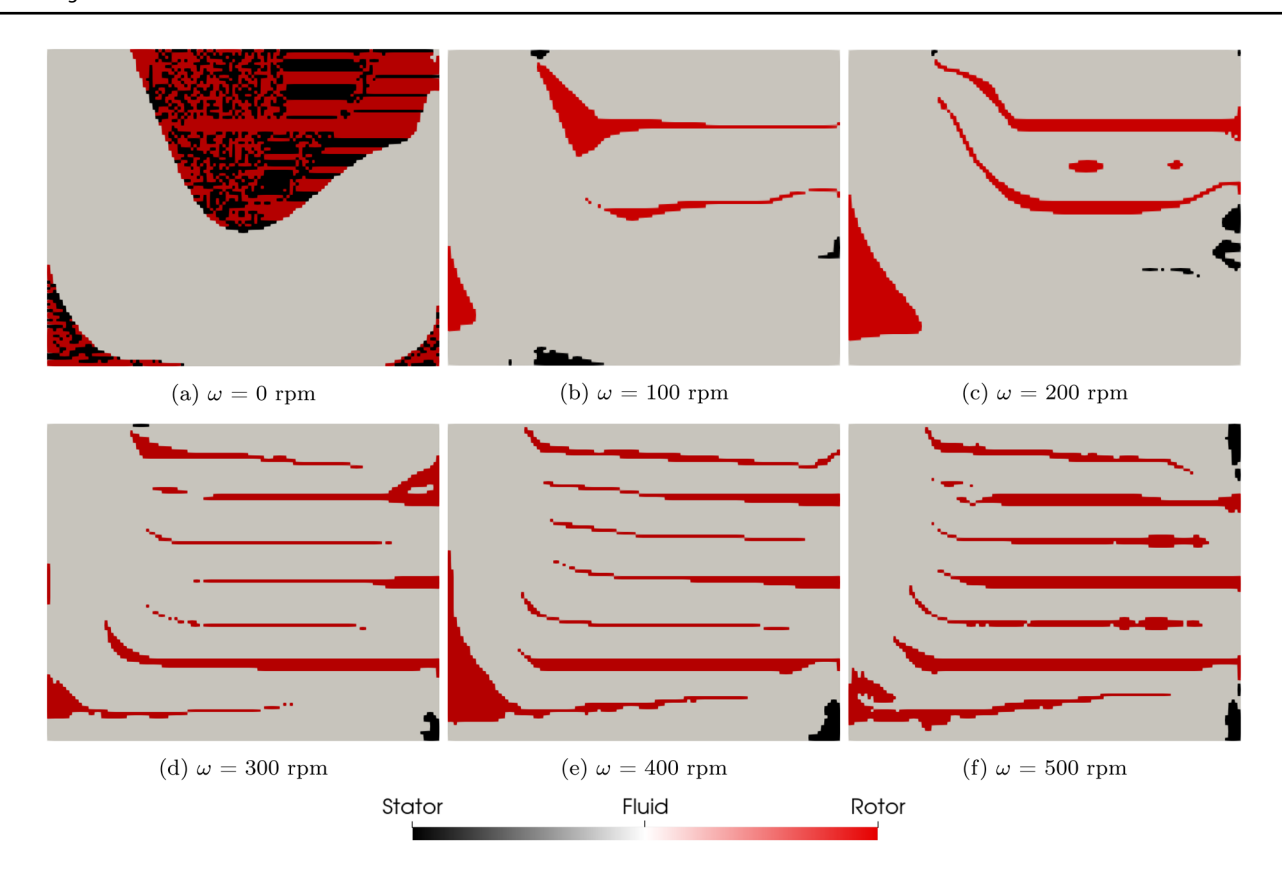


Fig. 16 Effect of the angular velocity in Tesla pump optimisation by starting from an initial guess with three rotor disks (Fig. 11g)

the objective function decreased instead of increasing due to linearization errors.

The velocity of rotor elements is zero in Fig. 13 because the reference frame is rotating with the shaft. Similarly, the velocity of stator elements increases with the r coordinate. The interaction between the rotor and stator at the upper and lower parts of the domain creates recirculation zones. These phenomena can also be observed by analysing the flow in the rz plane as presented by Fig. 14.

The topology optimisation results presented in Fig. 11 consider Eq. 9 to model solid elements. To check the accuracy of considering Darcy terms for stationary and rotating solid elements simultaneously, the result of Fig. 11i is

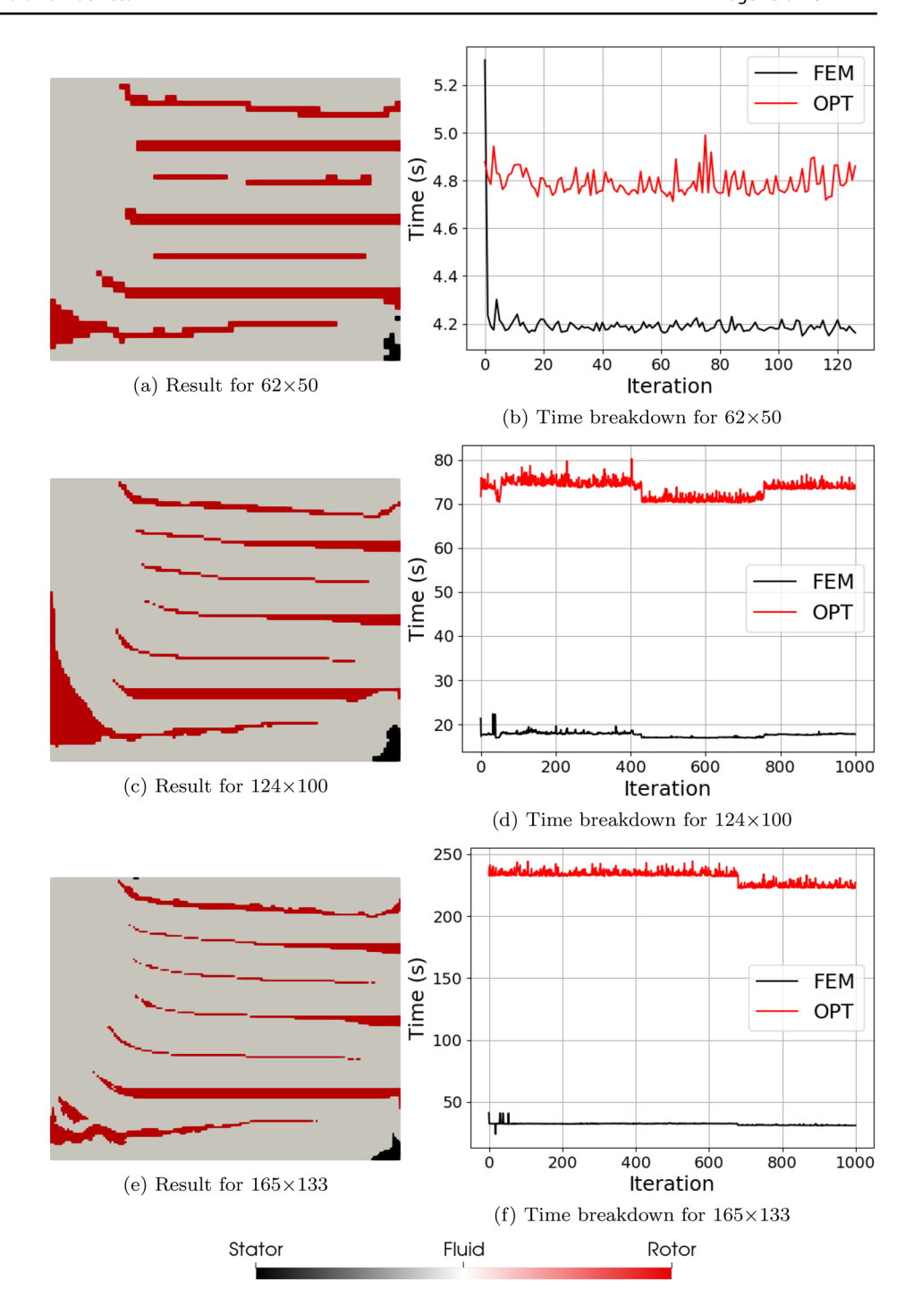
simulated in a pure fluid domain with Eq. 5 and the mesh from Fig. 15a. The velocity and pressure fields are presented in Fig. 15b and c, respectively. The fields of Fig. 13b and c are in accordance with Fig. 15b and c. Also, Table 4 shows that the pump power dissipation, the relative energy dissipation, the efficiency, and the pressure head present small differences which may be the result of different discretizations approaches such as triangular versus quadrilateral meshes and structured versus unstructured meshes. The local differences between the extended and the pure fluid fields are presented in Fig. 15d–g.

**Table 5** Tesla pump optimisation parameters for the evaluation of angular velocity effect (Fig. 16)

ω (rpm)	$J^0$ [W/(kg/m <sup>3</sup> )]	$J^*$ [W/(kg/m <sup>3</sup> )]	$\boldsymbol{\varPhi}_{R}^{0}\left(\mathrm{mW}\right)$	$\boldsymbol{\varPhi}_{R}^{*}\left(\mathbf{mW}\right)$	$\eta^0(\%)$	$\eta^*$ (%)	$H^0$ (mm)	<i>H</i> * (mm)
0	0.78	0.45	0.6	0.4	_	_	- 5.7	- 3.3
100	0.70	0.31	0.7	0.4	- 255%	- 730%	- 4.5	- 3.0
200	0.54	- 0.18	0.8	0.6	- 7%	- 266%	- 0.5	- 2.4
300	0.47	- 0.11	1.3	1.7	34%	48%	7.3	8.9
400	0.62	-0.84	2.3	3.0	46%	65%	19.8	23.2
500	0.96	<b>-</b> 1.77	4.0	6.6	51%	68%	37.4	35.3



Fig. 17 Time breakdown for different element sizes when starting the optimisation with three rotor disks (Fig. 11g)



# 4.1.1 Angular velocity effect

This section analyzes the angular velocity effect on the Tesla pump optimisation result. The proposed topology optimisation algorithm is run from angular velocities ranging from  $\omega = 0$  rpm to  $\omega = 500$  rpm by starting the optimisation with three rotor disks (Fig. 11g). The results are presented in Fig. 16.

For an angular velocity of  $\omega = 0$  rpm, the optimiser removes the starting disks and place all the material in the centre and right parts of the upper region according to Fig. 16a. The material is placed in the region of the design domain which poses fewer obstacles to the entering fluid. There are stator elements side-by-side with rotor elements as the angular velocity is zero. For  $\omega = 100$  rpm and 200 rpm, the initial configuration with three disks has negative



pressure head (Table 5) and the optimiser is not capable of designing a pump because the pressure head is negative. For angular velocities greater or equal to 300 rpm, the initial guess has positive pressure head and the optimiser increases the efficiency in all cases (Table 5).

#### 4.1.2 Time breakdown of the proposed algorithm

The proposed algorithm involves the addition of linear constraints to avoid the transition to the undesired state  $\alpha_i = 1$ and  $\beta_i = 1$ . One linear constraint is added per element, so the number of constraints is considerable and the optimisation time is increased in relation to the traditional TOBS approach. Therefore, an evaluation of the overall optimisation time is necessary. As the time required for running the FEM analysis and the optimisation routine dominate the overall time, only these steps are considered. Figure 17 presents the time breakdown (i.e., the time taken by each step) for element sizes 0.2 mm, 0.1 mm, and 0.075 mm, which results in discretizations of 62×50, 124×100, and 165×133 elements, respectively. The total time is 0.4 h for  $62 \times 50 (127)$ iterations), 29.8 h for 124×100 (1000 iterations), and 81.8 h for 165×133 (1000 iterations), which results in a mean iteration time of 12, 107, and 294 s/iteration approximately. The increase in the mean iteration time is mainly caused by the

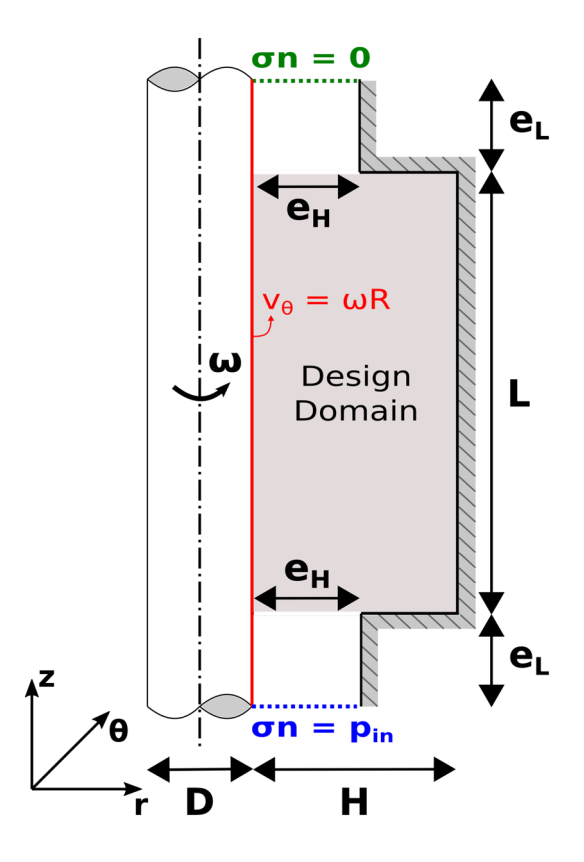


Fig. 18 Labyrinth seal design domain and boundary conditions



increase in the number of linear constraints (3100, 12400, 21975, respectively).

In Fig. 17, it is possible to observe that the integer linear optimisation procedure is the bottleneck of the overall optimisation for the proposed method. For an element size of 0.2 mm (Fig. 17a, b), the time for the FEM analysis and integer linear optimisation are similar. However, the duration of the optimisation routine is considerably higher for finer discretizations being ten times higher for an element size of 0.075 mm (Fig. 17e, f). Nevertheless, the time increase is not prohibitive for sufficiently fine discretizations as shown.

# 4.2 Labyrinth seal

In general, labyrinth seals are axisymmetric because they are applied to machines operating on high rotations in which balancing considerations are relevant. Therefore, most labyrinth seals can be modelled in 2D with cylindrical coordinates and axisymmetry around the rotating axis as illustrated by Fig. 18. The inlet is assigned to the lower port to emphasize that the upward flow (leakage) is undesired. Also, notice that for the labyrinth seal case the absolute reference frame is considered.

The oil SAE 15W-40 properties are also used in the labvrinth seal optimisation:  $\mu = 0.0146$  Pa.s and  $\rho = 835.2$ kg/m<sup>3</sup>. The default angular velocity used is  $\omega = 1000$  rpm unless otherwise noted. The geometric parameters chosen are: shaft diameter of D = 4 mm; design domain height of H= 10 mm, and auxiliary inlet and outlet channels height of  $e_H$ = 2 mm. The lengths of the design domain and of the auxiliary channels are determined by an aspect ratio parameter  $\delta$ = 1.6 such that  $L = \delta H$  and  $e_L = \delta e_H$ . The inlet pressure is  $p_{\rm in} = 1$  kPa and the outlet pressure is  $p_{\rm out} = 0$  Pa. The characteristic length is taken as the inlet/outlet channel height. The Reynolds number (based on the maximum velocity magnitude) is between 80 and 120 during the optimisation cases that consider  $\omega = 1000$  rpm. The Darcy number being used is  $10^{-11}$ . The optimisation problem is stated as the minimization of leakage at the outlet, the truncation error parameter is  $\zeta = 0.5\%$ , the minimum gap between rotor and stator  $g_{\min}$ is taken as the inlet height  $g_{\min} = e_H$  unless otherwise noted, the maximum number of iterations is  $n_{\text{max}} = 200$ , and the loop convergence criteria is  $n_{\text{loop}} = 20$ .

The design process started with an initial guess composed of only fluid elements and the optimisation result is a channel constricted up to the minimum-allowed gap between rotor and stator (Fig. 19a). Most of the constriction is promoted by projecting the rotor towards the stator. The bottom part of the seal has a smooth profile, and the top part presents some indentations. The velocity and pressure fields of result are presented in Fig. 19 with the rotor and stator contours displayed over each field. The rotor contour is presented in red or white, and the stator contour is presented

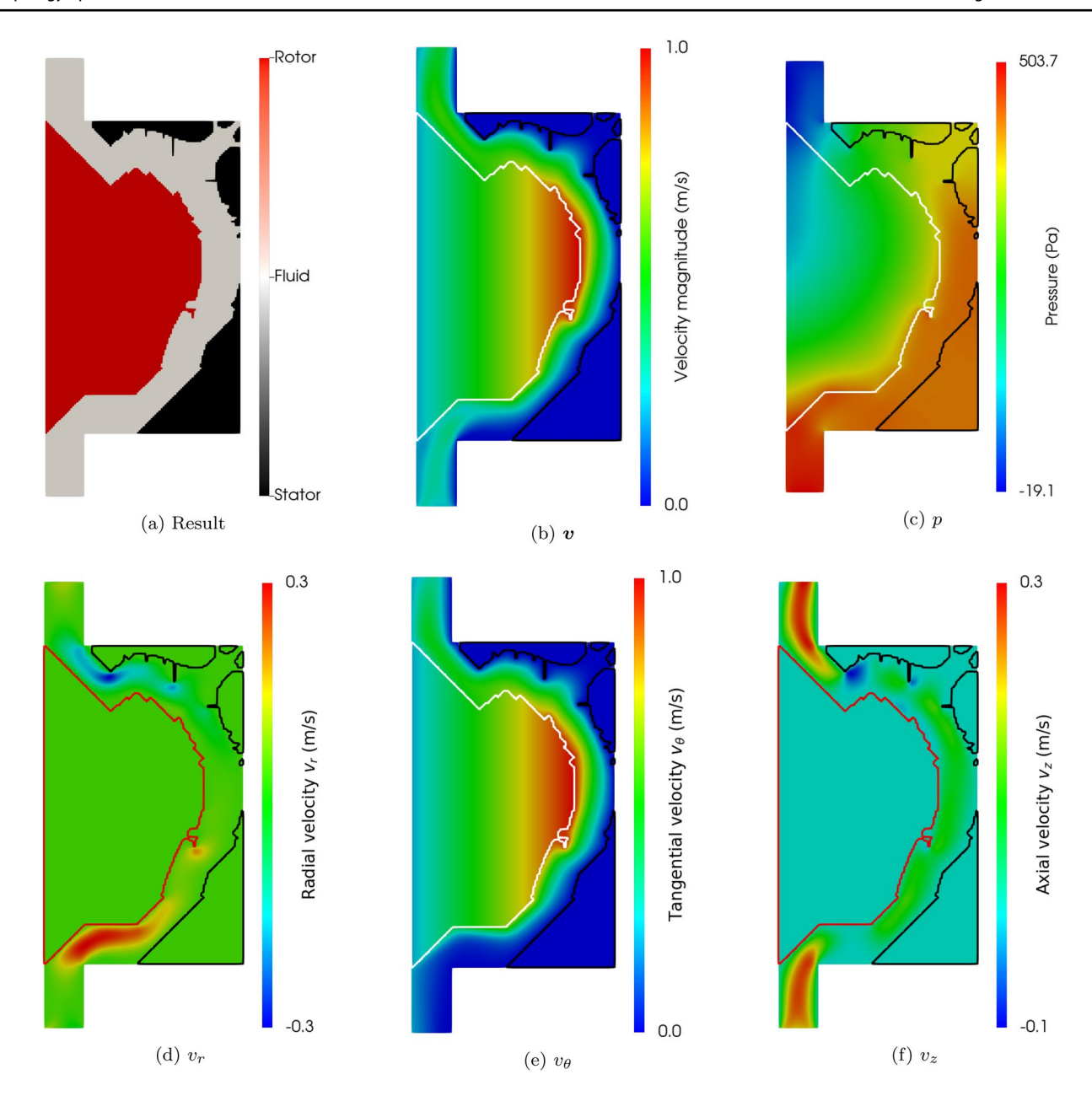


Fig. 19 Labyrinth seal result with velocity and pressure fields

in black. The velocity magnitude field (Fig. 19b) shows that the model is capable of assigning zero velocity to the stator phase and a purely tangential velocity to the rotor phase. Also, the rotor velocity increases with the r coordinate because the absolute reference frame is used. The pressure value (Fig. 19c) decreases from the inlet to the outlet, but most of the drop occurs in the upper part of the seal where the indentations are present.

In the labyrinth seal of Fig. 19a, the tangential velocity is orthogonal to the normal vectors of the inlet and outlet. Therefore, the leakage is the result of flow in the radial and axial directions. Figure 20 presents the flow in rz plane and

the streamlines. It is possible to observe that recirculation zones constrict the flow passage of the streamlines connecting the inlet to the outlet. Also, the fluid traverses the first half of the design domain attached to the rotor and the second part of the design domain attached to the stator.

The convergence data for the topology optimisation of the labyrinth seal is presented in Table 6. The number of iterations for reaching Fig. 19a is 105 and the objective function decreased to 31% of the initial value that considers a domain of only fluid elements.

The accuracy verification of the results from Fig. 19 is presented in Fig. 21 and Table 7. The velocity and pressure



142 Page 18 of 23 E. Moscatelli et al.

**Fig. 20** Velocity field in plane *rz* for the labyrinth seal result presented in Fig. 19a

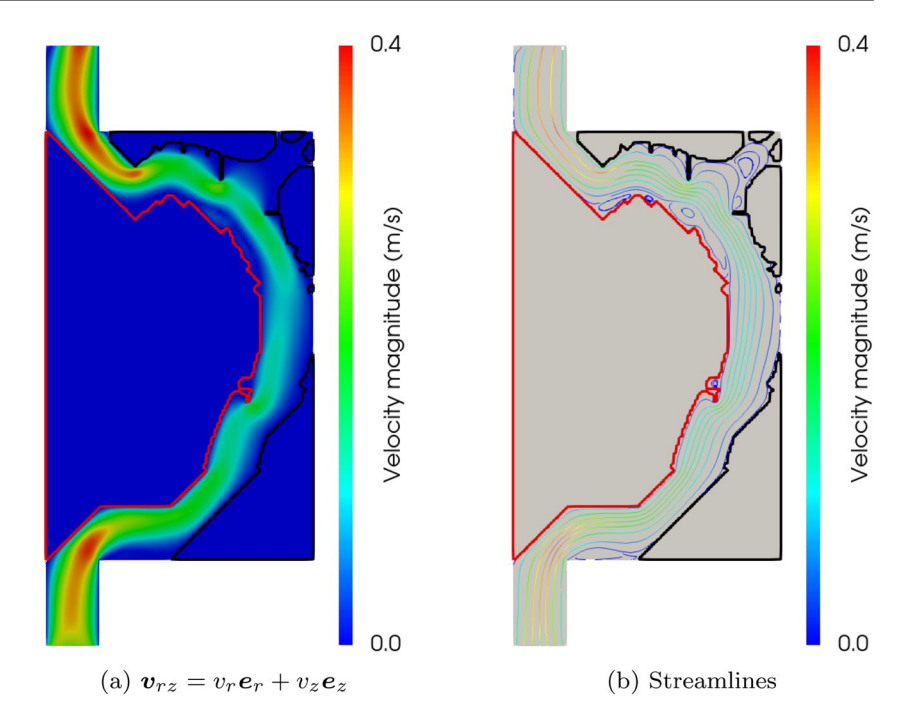


**Table 6** Convergence data for the topology optimisation of the labyrinth seal from Fig. 19a

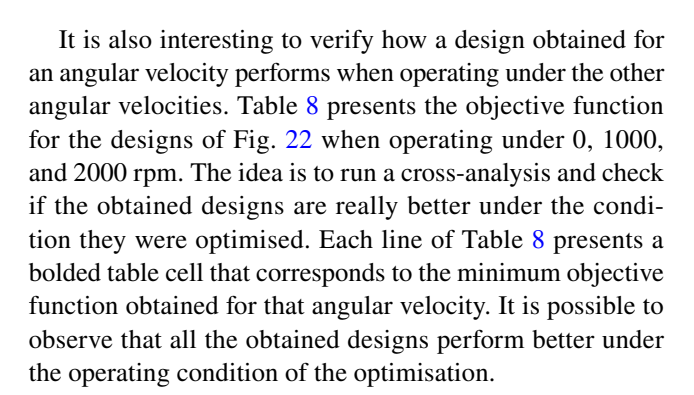
$n_{ m iter}$	$Q^{0}\left( \mathrm{g/s}\right)$	Q* (g/s)	$Q^*/Q^0(\%)$
105	21.2	6.5	31

The "0" superscripts indicate the values at the initial iteration and the "\*" superscripts indicate the optimised values

fields, the leakage, the pressure head and the energy dissipation calculated in the extended domain with Darcy terms are in accordance with the results obtained for the pure fluid domain without Darcy terms. The small differences are related to the meshes used for simulation.

# 4.2.1 Angular velocity effect

As the shaft angular velocity plays an important role in the fluid flow characteristics inside the labyrinth seal, it is important to analyze how the angular velocity of the rotor affects the optimisation results. Figure 22 presents the final topologies obtained for  $\omega=0$  rpm, 1000 rpm, and 2000 rpm. The result for  $\omega=0$  rpm (Fig. 22a) presents significant differences from the results obtained for  $\omega=1000$  rpm and 2000 rpm (Fig. 22b and c, respectively). In Fig. 22a, the rotor has a smaller diameter and a more irregular pattern. Figure 23 displays the behaviour of the convergence curves for the results presented in Fig. 22. The convergence curves obtained for the labyrinth seal optimisation are smooth and, in general, decrease monotonically.



#### 4.2.2 Initial guess effect

As the optimisation of the labyrinth seal through the minimization of leakage presents local minima, it is important to evaluate the effect of the initial guess on the optimisation result. In this section, the optimisation is started from designs with obstacles to fluid flow which are known as teeth in labyrinth seal literature and practice Flitney (2014). The initial guesses are built by distributing teeth uniformly over the design domain and by alternating the kind of teeth as rotor or stator. The obtained results are presented in Fig. 24 and Table 9.

One interesting feature of the results of Fig. 24 is the development of recirculation zones after each tooth. The recirculation zones can be observed in the streamlines of the velocity field (Fig. 25c). This feature is common to all the results from 24, and the recirculation zones are larger for Fig. 24a as the teeth had more space to grow. For the results in Fig. 24b and c, the recirculation zones have limited



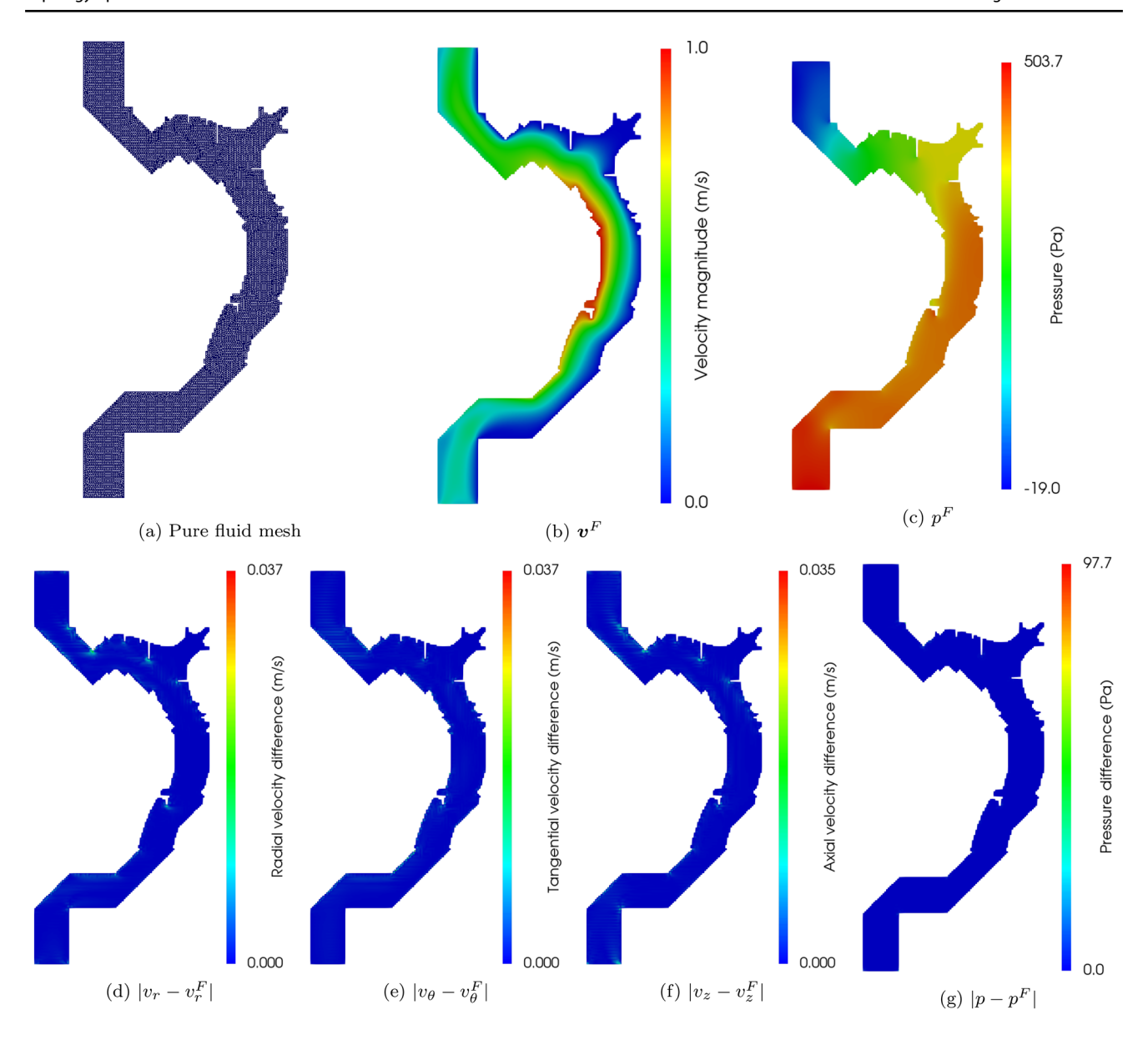


Fig. 21 Analysis of the labyrinth seal topology optimisation result in a pure fluid domain. a Pure fluid mesh, b Velocity magnitude for the pure fluid mesh, c Pressure for the pure fluid mesh, d Radial veloc-

ity difference,  ${\bf e}$  Tangential velocity difference,  ${\bf f}$  Axial velocity difference, and  ${\bf g}$  Pressure difference

**Table 7** Comparison of the labyrinth seal parameters obtained with a pure fluid domain and with an extended domain with Darcy terms for modelling solid phases

Domain	Equations	Figures	Q (g/s)	H(mm)	$\Phi$ (mW)
Extended	Equation 8	Figure 19	6.5407	- 56.356	13.451
Pure fluid	Equation 2	Figure 21	6.5337	- 56.358	13.453

space to grow due to the next tooth. The optimiser is free to remove all initial teeth, but it does not remove them because it would create a path to flow with increased leakage.

In Table 9, it is possible to observe that the initial objective function  $Q^0$  decreases with the number of teeth. The final values  $Q^*$  are also lower for more teeth, but the gain in  $Q^*/Q^0$  is reduced. The reduction indicates that the initial guess is closer to a local minimum when starting from a higher number of teeth.

#### 4.2.3 Gap size effect

The minimum gap size between rotor and stator is an important parameter in labyrinth seal design because the leakage decreases as the gap is reduced. However, there are practical



**142** Page 20 of 23 E. Moscatelli et al.

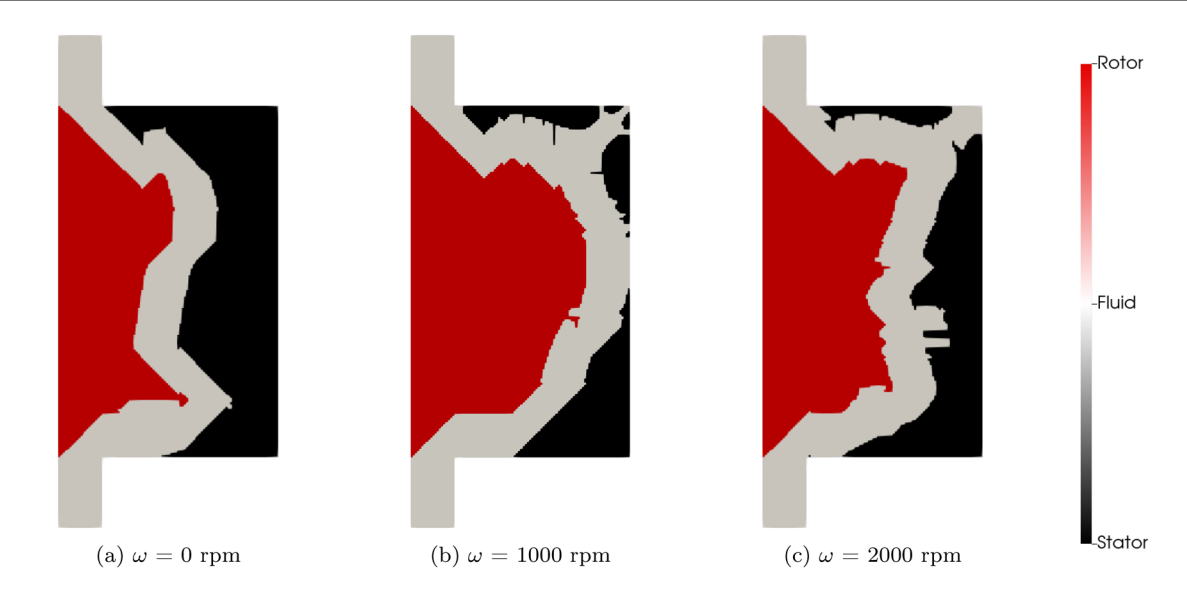


Fig. 22 Angular velocity effect in labyrinth seal optimisation for Re = 100

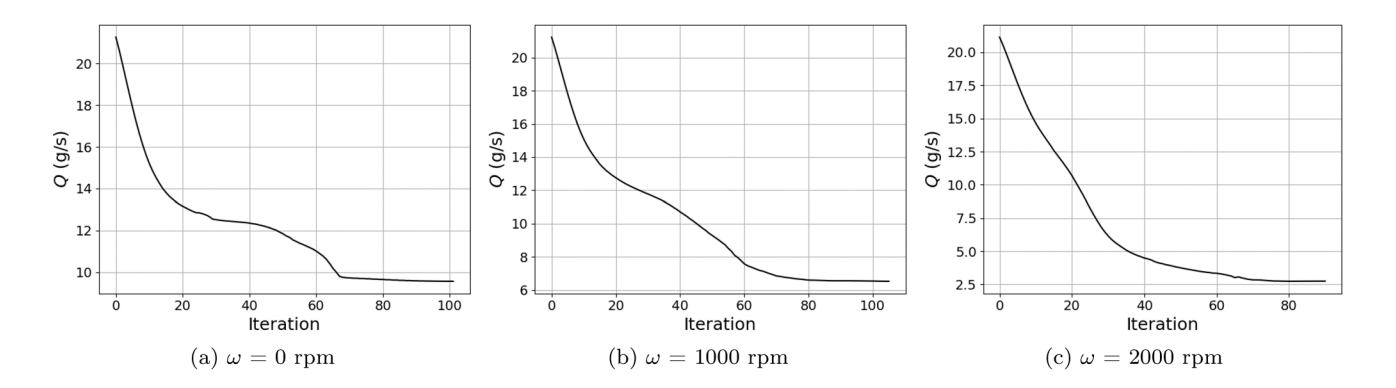


Fig. 23 Convergence curves of the objective function for the optimisation of labyrinth seal with different angular velocities (Fig. 22) and Re = 100

Table 8 Cross-analysis of the objective function (leakage) for the results of Fig. 22

Evaluation point	Leakage (g/s)					
	Design point					
$\omega$ (rpm)	0 rpm	1000 rpm	2000 rpm			
	(Figure 23a)	(Figure 23b)	(Figure 23c)			
0	9.6	10.1	10.4			
1000	7.1	6.5	7.0			
2000	2.8	3.3	2.7			

Each line presents a bolded table cell corresponding to the minimum value of objective function for that angular velocity

difficulties of operating labyrinth seals with small gap sizes because the rotor can brush the stator during transitory conditions such as when starting and stopping the rotating machine. Therefore, the gap size is an important design

**Table 9** Objective function reduction for the initial guess analysis from Fig. 24

	$n_{\mathrm{iter}}$	$Q^0$ (g/s)	Q* (g/s)	$Q^*/Q^0(\%)$
Figure 24a	94	10.8	6.2	57
Figure 24b	37	8.8	5.3	60
Figure 24c	44	5.3	4.0	75

The "0" superscripts indicate the values at the initial iteration and the "\*" superscripts indicate the optimised values

parameter and this work proposes an algorithm for controlling the gap size during optimisation. This section presents the effect of this algorithm by performing the optimisation with multiple  $g_{\min}/e_H$  relations and the result is presented in Fig. 26. As expected, the leakage decreases as the gap decreases. Also, lower gaps induce more irregular surfaces on the rotor and stator.



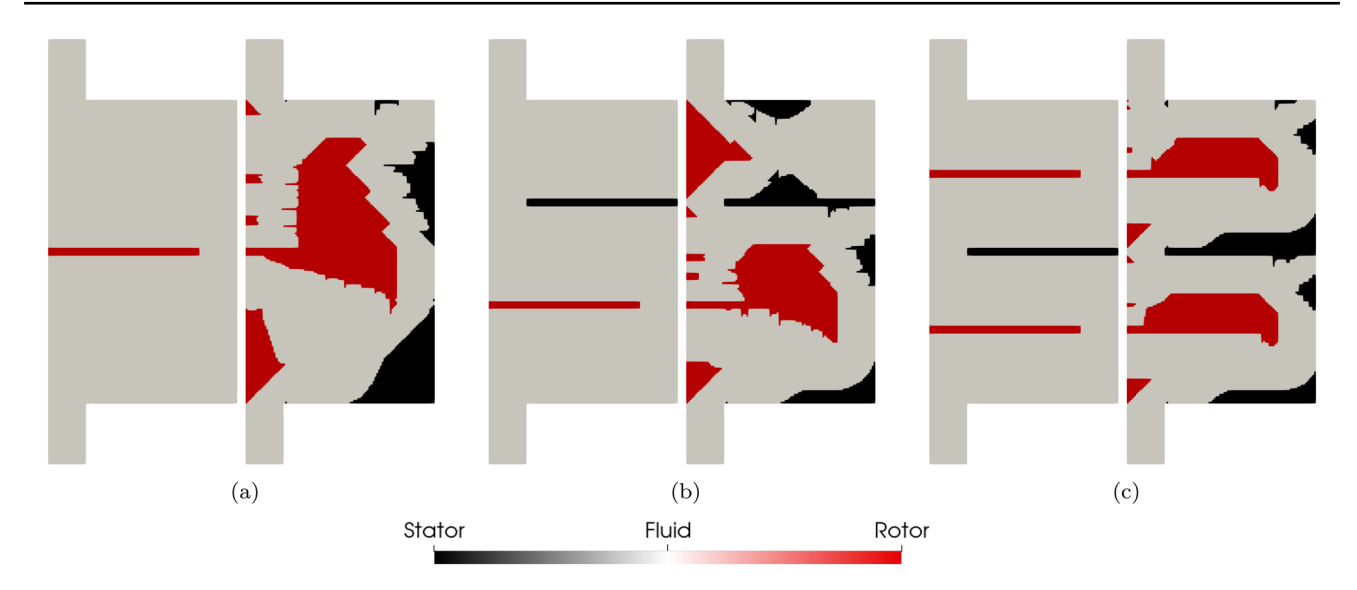


Fig. 24 Initial guess effect in labyrinth seal optimisation for  $\omega = 1000$  rpm. The initial guess is presented at left and the result at right for each item. a Initial guess with one tooth and result; b Initial guess with two teeth and result; c Initial guess with three teeth and result

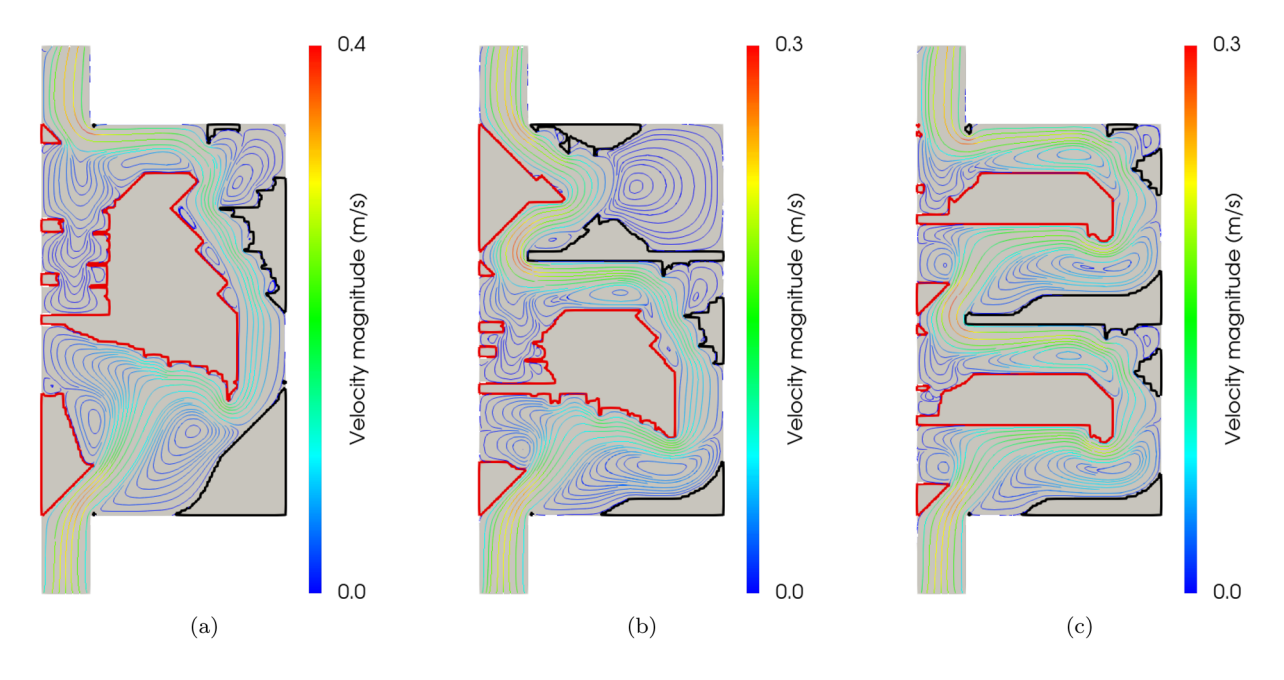


Fig. 25 Streamlines of the optimised results from Fig. 24

# **5 Conclusions**

This work presents a fluid flow topology optimisation algorithm capable of distributing solid material at different rotations. The algorithm has been successfully applied to two design problems: for a Tesla pump and a labyrinth seal. The algorithm is flexible to allow modifications for meeting other design constraints such as no floating islands and minimum

gap between rotor and stator. The effect of initial guess and rotor angular velocity is assessed for both problems.

For the Tesla pump problem, the objective function avoids the undesired contact between solid at different velocities without the introduction of additional constraints. However, for the labyrinth seal problem, it is necessary to modify the formulation to ensure minimum distance between solid elements at different velocities.



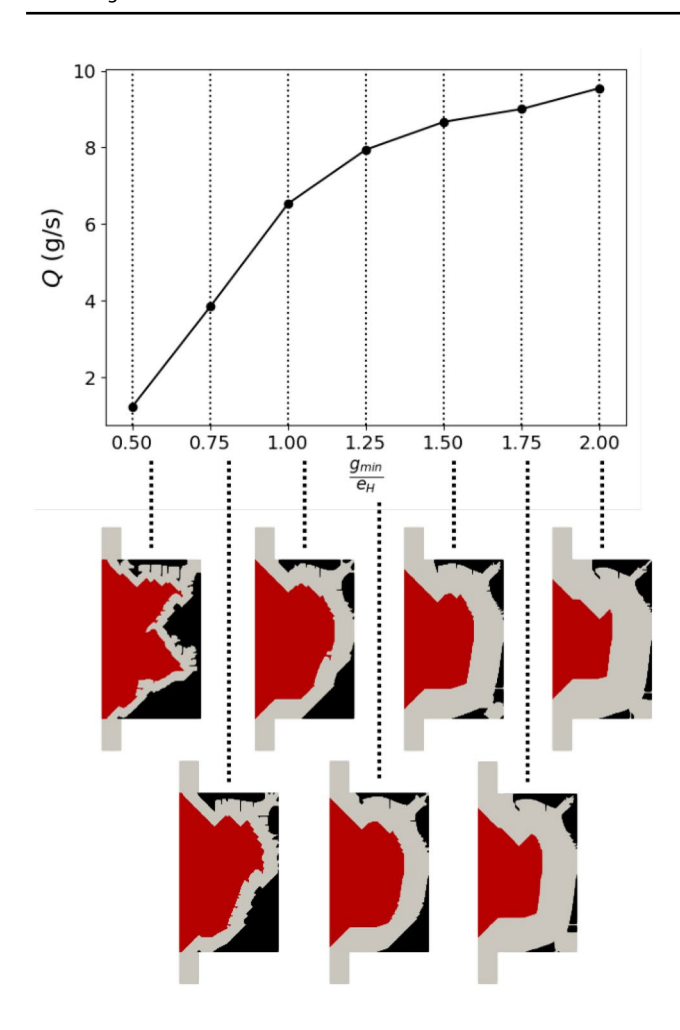


Fig. 26 Gap size effect in labyrinth seal optimisation for  $\omega = 1000$  rpm

For the labyrinth seal studied in this work, the gap reduction provides less leakage than creating a more tortuous path between rotor and stator. This can be associated with the low Reynolds number that has been considered.

As future research, the algorithm may be applied to fluid flow problems involving turbulent flow, compressible flow, non-Newtonian fluids, and other design problems such as compressors and fluidic diodes. Also, the proposed method may be explored for the design of heat exchangers and electric motors.

Funding This research was supported by CNPq (Brazilian Research Council) and FAPESP (Sāo Paulo Research Foundation). The authors thank the supporting institutions. The first author thanks FAPESP under Grant 2021/02340-0. The second author thanks the financial support of FAPESP under Grant 2017/27049-0. The fourth author thanks FAPESP under Grants 2018/05797-8 and 2019/01685-3. The last author thanks the financial support of CNPq (National Council for Research and Development) under Grant 302658/2018-1 and FAPESP under Grant 2013/24434-0. Also, we gratefully acknowledge the support of the RCGI—Research Centre for Greenhouse Gas

Innovation, hosted by the University of Sāo Paulo (USP) and sponsored by FAPESP—Sāo Paulo Research Foundation (2014/50279-4 and 2020/15230-5) and Shell Brasil, and the strategic importance of the support given by ANP (Brazil's National Oil, Natural Gas and Biofuels Agency) through the R&D levy regulation.

#### **Declarations**

Conflict of interest The authors declare that they have no conflict of interest

**Replication of results** To facilitate the replication of results, this paper discusses in detail the proposed formulation and provides the parameters for each presented result.

# References

Alexandersen J, Andreasen CS (2020) A review of topology optimisation for fluid-based problems. Fluids 5(1):29. https://doi.org/10.3390/fluids5010029

Alnæs M, Blechta J, Hake J, Johansson A, Kehlet B, Logg A, Richardson C, Ring J, Rognes ME, Wells GN (2015) The FEniCS project version 1.5. Arch Numer Softw. https://doi.org/10.11588/ANS. 2015.100.20553

Alonso DH, de Sá LFN, Saenz JSR, Silva ECN (2018) Topology optimization applied to the design of 2D swirl flow devices. Struct Multidisc Optim 58(6):2341–2364. https://doi.org/10.1007/s00158-018-2078-0

Alonso DH, de Sá LFN, Saenz JSR, Silva ECN (2019) Topology optimization based on a two-dimensional swirl flow model of Teslatype pump devices. Comput Math Appl 77(9):2499–2533. https://doi.org/10.1016/j.camwa.2018.12.035

Balay S, Abhyankar S, Adams MF, Brown J, Brune P, Buschelman K, Dalcin L, Dener A, Eijkhout V, Gropp WD, Kaushik D, Knepley MG, May DA, McInnes LC, Mills RT, Munson T, Rupp K, Sanan P, Smith BF, Zampini S, Zhang H, Zhang H (2021a) PETSc Web page. https://petsc.org/release/#citing-petsc

Balay S, Abhyankar S, Adams MF, Brown J, Brune P, Buschelman K, Dalcin L, Dener A, Eijkhout V, Gropp WD, Kaushik D, Knepley MG, May DA, McInnes LC, Mills RT, Munson T, Rupp K, Sanan P, Smith BF, Zampini S, Zhang H, Zhang H (2021b) PETSc users manual. Technical report ANL-95/11—revision 3.15. Argonne National Laboratory, Lemont

Bendsøe MP, Sigmund O (1999) Material interpolation schemes in topology optimization. Arch Appl Mech (Ingenieur Archiv) 69(9–10):635–654. https://doi.org/10.1007/s004190050248

Borrvall T, Petersson J (2003) Topology optimization of fluids in stokes flow. Int J Numer Methods Fluids 41(1):77–107. https://doi.org/ 10.1002/fld.426

Farrell PE, Ham DA, Funke SW, Rognes ME (2013) Automated derivation of the adjoint of high-level transient finite element programs. SIAM J Sci Comput 35(4):C369–C393. https://doi.org/10.1137/120873558

Flitney R (2014) Seals and sealing handbook. Butterworth-Heinemann, Oxford

Høghøj LC, Nørhave DR, Alexandersen J, Sigmund O, Andreasen CS (2020) Topology optimization of two fluid heat exchangers. Int J Heat Mass Transf 163:120543. https://doi.org/10.1016/j.ijhea tmasstransfer.2020.120543

Kobayashi H, Yaji K, Yamasaki S, Fujita K (2021) Topology design of two-fluid heat exchange. Struct Multidisc Optim 63(2):821–834. https://doi.org/10.1007/s00158-020-02736-8



- Mitusch S, Funke S, Dokken J (2019) Dolfin-adjoint 2018.1: automated adjoints for FEniCS and firedrake. J Open Source Softw 4(38):1292. https://doi.org/10.21105/joss.01292
- Okubo CM, Kiyono CY, Sá LF, Silva EC (2021) Topology optimization applied to 3D rotor flow path design based on the continuous adjoint approach. Comput Math Appl 96:16-30. https://doi.org/ 10.1016/j.camwa.2021.05.006
- Romero J, Silva E (2014) A topology optimization approach applied to laminar flow machine rotor design. Comput Methods Appl Mech Eng 279:268-300. https://doi.org/10.1016/j.cma.2014.06.029
- Sá LFN, Romero JS, Horikawa O, Silva ECN (2018) Topology optimization applied to the development of small scale pump. Struct Multidisc Optim 57(5):2045-2059. https://doi.org/10.1007/ s00158-018-1966-7
- Sá LFN, Okubo CM, Sá AN, Silva ECN (2022) Continuous boundary condition propagation model for topology optimization. Struct Multidisc Optim. https://doi.org/10.1007/s00158-021-03148-y

- Sivapuram R, Picelli R (2018) Topology optimization of binary structures using integer linear programming. Finite Elem Anal Des 139:49-61. https://doi.org/10.1016/j.finel.2017.10.006
- Souza BC, Yamabe PVM, Sá LFN, Ranjbarzadeh S, Picelli R, Silva ECN (2021) Topology optimization of fluid flow by using integer linear programming. Struct Multidisc Optim. https://doi.org/10. 1007/s00158-021-02910-6
- Tawk R, Ghannam B, Nemer M (2019) Topology optimization of heat and mass transfer problems in two fluids-one solid domains. Numer Heat Transf B 76(3):130-151. https://doi.org/10.1080/ 10407790.2019.1644919

Publisher's Note Springer Nature remains neutral with regard to jurisdictional claims in published maps and institutional affiliations.

